NASA Contractor Report 191605

Effective Conductivity of Wire Mesh Reflectors for Space Deployable Antenna Systems

William A. Davis
Virginia Polytechnic Institute and State University, Blacksburg, Virginia

Contract NAS1-18471
March 1994

National Aeronautics and
Space Administration
Langley Research Center
Hampton, Virginia 23681-0001

EFFECTIVE CONDUCTIVITY OF WIRE MESH REFLECTORS FOR SPACE DEPLOYABLE ANTENNA SYSTEMS

Final Report

ABSTRACT

This report summarizes efforts to characterize the measurement of conductive mesh and smooth surfaces using proximity measurements for a dielectric resonator. The resonator operates in the HEM_{11} mode and is shown to have an evanescent field behavior in the vicinity of the sample surface, raising some question to the validity of measurements requiring near normal incidence on the material. In addition, the slow radial field decay outside of the dielectric resonator validates the sensitivity to the planar supporting structure and potential radiation effects. Though these concerns become apparent along with the sensitivity to the gap between the dielectric and the material surface, the basic concept of the material measurement using dielectric resonators has been verified for useful comparison of material surface properties. The properties, particularly loss, may be obtained by monitoring the resonant frequency along with the resonator quality factor (Q), 3 dB bandwidth, or the midband transmission amplitude. Comparison must be made to known materials to extract the desired data.

TABLE OF CONTENTS

CHAPTER 1

INTRODUCTION

1.1 INTRODUCTION

This report summarizes the research effort to evaluate the potential for using a dielectric resonator in the vicinity of a planar, conducting, material sample to determine the loss properties of the sample. This introduction and resultant conclusions summarize the extensive work documented in the appendix and submitted as a thesis for the MS degree at Virginia Tech. The thesis develops the theory for approximate analysis of dielectric resonators based on a review of a variety of methods expounded in the literature. The technique of Itoh [4] provides useful results, but is found to be a bit too approximate for the problem at hand. A full problem development could have been pursued, but was not felt to be necessary for the justification goal of the report. In order to obtain useful results, a middle-of-the-road approach was taken which addressed some of the techniques suggested by Itoh and added a more complete description to the capped terminations of the resonator. In particular, the consideration of bringing a planar material within the proximity of a planar end of the resonator is included in the report.

1.2 BASIC APPROACH

To attack the problem at hand (see Fig. 2.1 of Appendix), the resonator was first considered to be a dielectric waveguide. Thus, the properties of a circular dielectric waveguide were developed for an infinite dielectric rod. The properties of the rod analysis were not fixed, but were developed for use in an iterative process as would be required for the determination of

the dielectric resonator properties, those of a truncated dielectric rod. Several classic cases were considered in order to provide validation to the code. The validation simply involved the determination of the fields and longitudinal propagation constant of the dielectric rod for different modes as expected from the literature.

The next step in the development was the truncation of the dielectric rod to represent a circular dielectric resonator. The ends of the resonator were modeled as simple connections to open space. The boundary conditions at the ends were approximated by either the electric field or magnetic field mode dominance characteristic of hybrid dielectric waveguide modes. This boundary condition was thus represented by a reflection coefficient which was iteratively added to the dielectric rod waveguide delay to obtain a round-trip delay having a multiple of 360° phase shift. The iterative process consisted of searching for the complex frequency at which the proper phase shift occurred. In addition, the properties of the reflection coefficient magnitude and the dielectric rod propagation loss directly impact on the imaginary part of the complex frequency and thus the dielectric Q of the resonator. Thus the Q for a particular mode may be determined and used in an estimate of the loss.

To obtain the material loss estimate, the reflection coefficient at the end of the resonator adjacent to the planar sample was modified to include the sample energy absorption. Thus the overall modification in the resonator Q was evaluated. Sample results for the analysis in the presence of a lossy material sample is included in Section 3.5 of the appendix.

CHAPTER 2

CONCLUSIONS

This report has summarized the potential for using a dielectric resonator in the vicinity of a planar, conducting, material sample to determine the loss properties of the sample. The theory for approximate analysis of dielectric resonators is reviewed, incorporating a variety of methods. The technique of Itoh [4] provides the most straight forward approach to the problem, but was found to be a bit too approximate for the problem at hand. Itoh's approach was extended to address a more complete description with a truncated circular resonator. An additional extension included the ability to bring a planar material within the proximity of the planar end of the resonator.

The resonator was first treated as an infinite dielectric waveguide. The properties of the rod analysis were iteratively used in a program along with an estimate of the reflection properties at the resonator ends to determine the basic complex frequency of the dielectric resonator, the imaginary part of the resonate frequency directly providing an estimate of the resonator Q, quality factor. The ends of the resonator were initially modeled as simple connections to open space. The boundary conditions at the ends were approximated by either the electric field or magnetic field mode dominance characteristic of hybrid dielectric waveguide modes. This boundary condition was thus represented by a reflection coefficient which was iteratively added to the dielectric rod waveguide delay to obtain a multiple of 360° phase shift. The iterative process consisted of searching for the complex frequency at which the proper phase shift occurred. The imaginary part of the complex frequency was used to determine the resonator Q and thus the resonator loss.

The properties of planar materials adjacent to the resonator end were used to evaluate the effects of the resonator loss estimate by modifying the reflection coefficient at the end of the resonator adjacent to the planar sample to include the sample energy absorption. Thus the overall modification in the resonator Q was evaluated. Sample results for the analysis in the presence of a lossy material sample indicate a change in the resonator frequency and Q, thus providing support for the use of the corresponding resonator transmission amplitude for comparison of material properties of materials set adjacent to the resonator end. It is important to recognize that the only information which is directly available is a comparison with other samples. Thus, several known materials must be used for comparison in order to calibrate the effective measurements used in the system. The data is found to be very sensitive to outside influences and sample placement distances. Extreme care must be taken in the placement and surrounding environment of the measurement system in order to obtain repeatable and useful results. If adequate precautions are taken, the results obtained from several material measurements will provide useful information on the quality of a mesh conductor used for the reflector of a space deployable antenna system.

APPENDIX

MS Thesis

"Dielectric Resonator in the Presence of a Lossy Conductor"

by

Scott B. Johnston

Bradley Department of Electric Engineering

Virginia Polytechnic Institute and State University

Blacksburg, Virginia

DIELECTRIC RESONATOR IN THE PRESENCE

OF A LOSSY CONDUCTOR

by

Scott B. Johnston

Dr. William A. Davis, Chairman

Electrical Engineering

(ABSTRACT)

This thesis develops a method for obtaining the complex resonant frequency of a post dielectric resonator in the presence of a lossy conductor. A full field analysis is performed on an infinite dielectric rod from which the complex propagation constant and modal solutions are found. Using a single dominant mode (HEM_{11}), the boundary conditions at the end of the resonator are enforced, to obtain a complex reflection coefficient. Using the propagation constant from the infinite dielectric rod and the reflection coefficient derived from considering the dielectric-air interface at the resonator ends, a two dimensional search is performed to find the complex frequency for which the gain/phase criterion of the resonator is satisfied. In the final step, boundary conditions are enforced for a lossy conductor at a distance Δz from the dielectric which yields the objective -- the complex resonate frequency of a post dielectric in close proximity of a lossy conductor.

Acknowledgement

I would like to express my appreciation to Dr. Davis for the opportunity to work on this project. With his assistance I have learned much about the principles of electro-magnetics. In addition through Dr Davis's patience and persistence I have become aware of the importance of a sound understanding of basic principles and complete, thorough development. I extend my gratitude to the other committee members, Dr. Besieris and Dr. Jazi, who were invaluable as teachers and generous with their time in helping me better understand the basic principles on which this thesis is based. Finally, I would like to recognize NASA, Langley for their support of this project.

Table of Contents

Chapter 1

Introduction

It was recognized in the 1960's that high-Q dielectrics held high promise in the area of microwave electronics. The advent of temperature-stable materials such as barium tetratitanate, allowed dielectrics to be used in microwave systems such as oscillators, filter banks, and multiplexers. Following the temperature-stability breakthrough numerous papers have been written on both material aspects of dielectrics and the electro-magnetic field models of dielectric resonators. Various scientists have devised schemes using high-Q post dielectric resonators between two conductive shields to measure physical properties such as dielectric constant and loss tangent of the dielectric at frequencies of interest [1;3]. The modeling work in this thesis will reverse the scheme by using a fully characterized dielectric to determine the electrical conductivity of a single conductor in close proximity of the post dielectric resonator.

The work of this thesis is similar to work by other authors [4;-;7], in the attempt to derive the field distribution and to determine the resonant frequency of the post dielectric resonator. Itoh [4], considering the TE_{01} mode, makes several approximations about the field configuration that yield a simple numeric method for determining the fields in and around the post dielectric and the resulting resonant frequency. Due to the similarity of basic principles of Itoh's work and this thesis, Chapter 2 reviews his paper, "New Method for Computing the Resonant Frequencies of Dielectric Resonators" [Itoh,4]. In another paper, Marek Jaworski [7] achieves similar results to Itoh's by applying a Green's function in an

elegant, but rigorous mathematical model of the dielectric resonator. While Itoh's and Jaworski's works address general characteristics of the dielectric resonator, this thesis considers a very specific problem: the complex resonant frequency of a post dielectric resonator of specific profile in close proximity of a lossy conductor.

The goals of this thesis are threefold: first, derive the electro-magnetic fields associated with the specific experimental setup to facilitate a better understanding of how the evanescent fields couple to the surrounding experimental setup; second, develop a method of calculating the complex resonant frequency; and third, develop computer models to aid in the determination of the conductivity of the material being used as the ground plate.

Chapter 2 presents background information pertinent to this work, introduces the resonator system under study, and outlines the method of development employed to achieve the three goals of this thesis. Chapter 3 develops the resonator system in the four following stages: first, the field configuration for the infinite dielectric waveguide is derived; second, the fields and the resonant frequency for a free space resonator are determined; third, the fields and resonant frequency for the resonator in the presence of a perfect conductor are derived; and finally, the fields and resonant frequency for the resonator in the presence of a lossy conductor are derived. The final chapter provides conclusions and recommendations.

Chapter 2

Background

2.1 Introduction of the Experiment

The experimental setup under consideration is shown in Fig. 2.1a. The experiment has been devised to determine the electrical conductivity of the mesh used to shield the dielectric from above. The measurable parameters of the experiment are the S parameters of the system. Of interest in this experiment is the one port parameter s_{11} which is return loss and the two port parameter s_{12} which is insertion loss. At a resonant frequency, power will be coupled from one probe to the other. Resonance will be noted on the network analyzer when the return loss increases and the insertion loss decreases. The two probes of the network analyzer are positioned to couple lightly into the dielectric but not to couple significantly to each other [9].

The post dielectric rod is supported by rexolyte from below and the conducting material of interest in close proximity above. The rexolyte has a relative permittivity approximately equal to one and the thickness is assumed to be large compared to the penetration of the evanescent fields. The four conductor supports are far enough away from the dielectric not to couple into the radial evanescent fields. The validity of these assumptions will be verified in Section 3.3.

Section 3.3 will show that the placement of the conductor should be within 0.5 cm of the

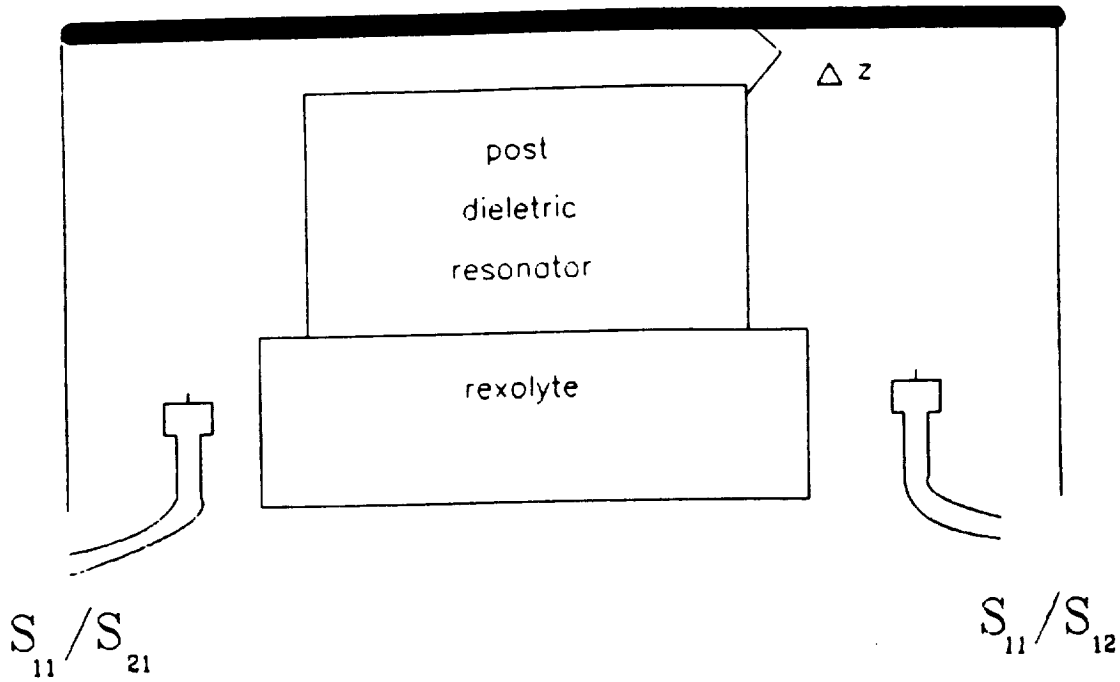

Figure 2.1a NASA's post dielectric resonator system

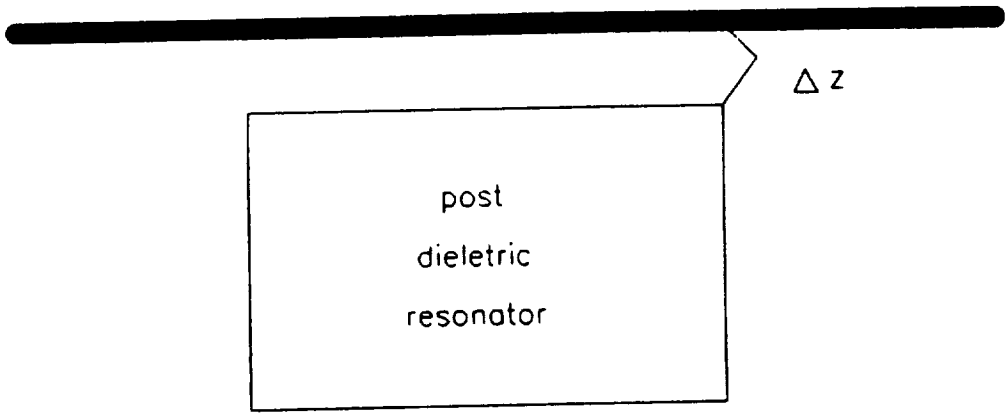

Figure 2.1b NASA's experiment after approximation

dielectric. One method of quantifying the mesh conductivity involves using several known conductors as the ground plate. The mesh pressed directly against the dielectric provides for easier analysis, but as will be seen in Section 3.4, is not necessary. What is necessary is a mechanism to provide a repeatable way to alternate conductors while maintaining the same air gap distance between the conductor and the dielectric. If the measurement for one conductor is made with zero air gap, the measurements for all other conductors should also be made with zero air gap.

As stated in Chapter 1, the first goal of this thesis is to derive the fields in and around the dielectric of Fig. 2.1a. The complexity of the derivation is greatly simplified by making the following assumptions:

1) infinite conductor

2) each region source free

3) conductor and dielectric system in free space.

These assumptions reduce the system under consideration to that of Figure 2.1b. Although the system of Fig. 2.1b is simpler than the experimental setup, the configuration of the system remains non-separable. In contrast to the infinite cylindrical metal waveguides, boundary conditions of the resonator must be satisfied at the cylindrical sides and at both ends. The problem of the non-separable geometry will be addressed in Chapter 3.

Before reviewing the applicable literature, notation used in the remainder of the thesis is defined as follows:

S – complex resonant frequency given by $S = \zeta + j\omega$

ω = resonant frequency

ζ = damping factor

k_z = complex propagation constant given by $k_z = \beta - j\alpha$

α = attenuation constant

k_o = free space propagation constant

ϵ_r = complex relative permittivity of the dielectric

σ = conductivity of the conductor

2.2 Literature Review

In the paper "New Methods for Computing the Resonant Frequencies of Dielectric Resonator" [4], Itoh makes several assumptions about the TE_{01} electromagnetic fields of the post dielectric resonator. Itoh's post dielectric resonator is shown in Fig. 2.2a. The assumptions made in Itoh's paper are:

1) majority of stored energy is in dielectric

2) fields decay exponentially at the ends

3) small amount of energy in fringe area, regions 5 and 6 of Fig. 2.2b.

4) lossless dielectric ($\epsilon_r = \epsilon_r - j0$)

5) lossless conductor ($\sigma \to \infty$) at $z = -t$

Itoh's assumptions of a perfect dielectric and a perfect conductor result in a resonant frequency that is purely real. Using these assumptions, it is sufficient to match the fields that are tangent to the boundaries. Itoh assumes the fields in the four regions for an unknown z_0 are

$$H_z = \begin{cases} A_1 \sin\beta(z-z_0) J_0(h\rho) & \text{region 1} \quad (2.1a) \\ A_2 \sin\beta(z-z_0) K_0(p\rho) & \text{region 2} \quad (2.1b) \\ A_3 \exp[-\gamma(z-L) J_0(h\rho) & \text{region 3} \quad (2.1c) \\ A_4 \sinh\zeta(z+t) J_0(h\rho) & \text{region 4} \quad (2.1d) \end{cases}$$

where

$$\beta^2 = \epsilon_{r1} k_0^2 - h^2 = k_0^2 + p^2$$

$$\gamma^2 = h^2 - k_0^2$$

$$\zeta^2 = h^2 - \epsilon_{r2} k_0^2$$

$$k_0 = \omega_0 \sqrt{\epsilon_0 \mu_0}.$$

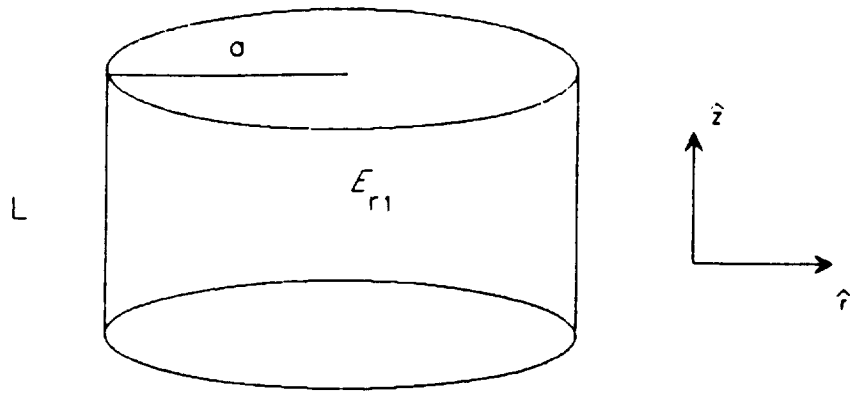

Figure 2.2a Itoh's dielectric resonator

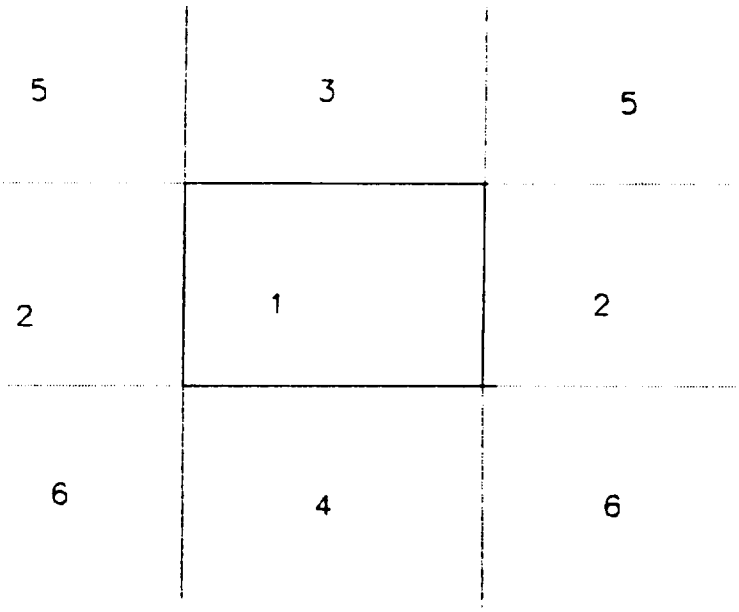

Figure 2.2b Six regions of the resonator

The relative dielectric constant is ϵ_{r2} and the thickness of the material below the resonator is t. The fields in the regions five and six are assumed to be zero, or at least negligible. The remaining two components E_ϕ and H_ρ are uniquely specified once H_z is determined and are derived in terms of H_z in Appendix A. Matching tangential components at the dielectric boundary, performed in appendix B, leaves two eigenvalue equations

$$\frac{k_{1\rho} J_o'(k_{1\rho}a)}{J_o(k_{1\rho}a)} = \frac{jk_{2\rho} K_o'(jk_{2\rho}a)}{K_o(jk_{2\rho}a)} \tag{2.2a}$$

$$\beta L = \tan^{-1}\left(\frac{\gamma}{\beta}\right) + \tan^{-1}\left(\frac{\zeta}{\beta}\coth\zeta t\right) . \tag{2.2b}$$

For the dielectric resonating in free space, t→∞, 2.2b becomes

$$\beta \tan\left(\frac{\beta L}{2}\right) = \gamma. \tag{2.2c}$$

Given a free space dielectric with height of $L = 0.508$ cm, radius of $a = 0.63$ cm, and $\epsilon_r = 40$, numerical methods were used to solve the coupled Eq. 2.2a and 2.2c resulting in a resonant frequency of

$$f_r = 4.36\ Ghz .$$

Itoh's work results in a quick method for determining the electromagnetic fields and resonant frequency of TE_{0m} modes. Itoh's method is not mathematically rigorous; however, his method for determining fields and resonant frequency is suitable for perturbation studies. Possible perturbations include distance between ground plane and dielectric, changes in the dielectric constant, and changes in the physical profile of the dielectric. What the model does not provide is a way to calculate hybrid modes or to make provisions for a conductor with finite conductivity. Methods addressing these two anomalies will be developed in Chapter 3.

2.3 PMC Dielectric Resonator

In this section the free space resonator, shown in Fig. 2.3a, is analyzed using the assumptions of a perfect magnetic conductor, PMC. This assumption has been a celebrated method used to determine electromagnetic fields, the propagation constant of dielectric waveguides, and the resonant frequency of dielectric resonators [10]. The PMC model assumes that the tangential magnetic fields are zero at the dielectric-air boundary. This simplifying assumption produces numerical solutions with errors as high as 25%. For example, it will be shown by a more rigorous method used in Section 2.2 and Chapter 3 that the PMC method gives a resonant frequency that is 20% lower than the actual TE_{011} resonant frequency. The PMC method provides however a convenient "back of the envelope" procedure for the quick determination of propagation constant and resonant frequency.

The PMC derivation of TE_{nmp} modes begins with the solution of the Helmholtz's wave equation in a non-magnetic medium. The electric potentials that satisfy Helmholtz's equation in region one and region two (Fig. 2.3b) are given by

$$\Psi^{E}_{1_{nm}} = A\ B^{1}_{n}(k_{1\rho}\rho)(C_1\ cos(k_z z) + D_1\ sin(k_z z))\ e^{jn\phi}\ ,\quad \rho < a \tag{2.3}$$

and

$$\Psi^{E}_{2_{nm}} = BB_{n}(k_{2\rho}\rho)(C_2\ cos(k_z z) + D_2\ sin(k_z z))\ e^{jn\phi}\ ,\quad \rho > a \tag{2.4}$$

where $B^{1,2}_{n}$ denotes a general Bessel function of the nth order. The subscript m denotes the mth solution for a particular n. The separation equation for the two regions are

$$k_1^2 = k_{1\rho}^2 + k_z^2 = \omega_o^2\,\mu_o\epsilon_r\epsilon_o \tag{2.5}$$

and

$$k_2^2 = k_{2\rho}^2 + k_z^2 = \omega_o^2\,\mu_o\epsilon_o. \tag{2.6}$$

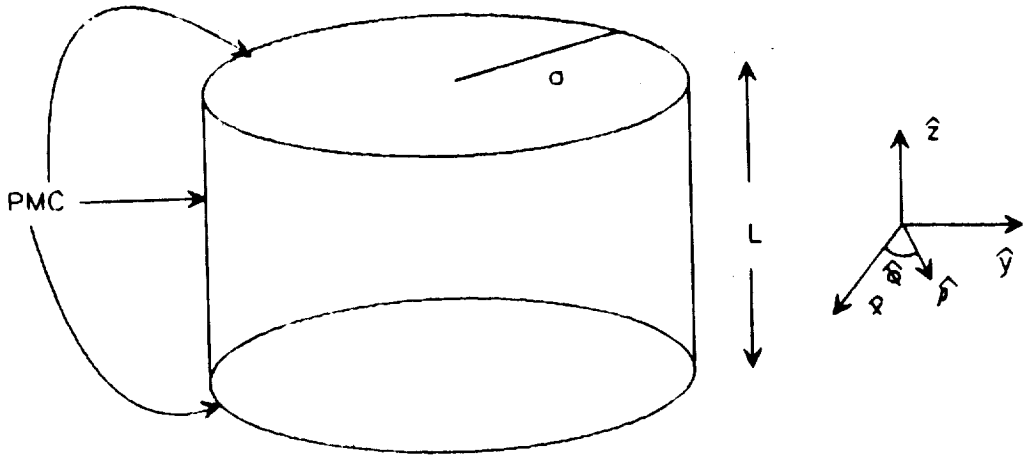

Figure 2.3a PMC, Perfect Magnetic Conductor

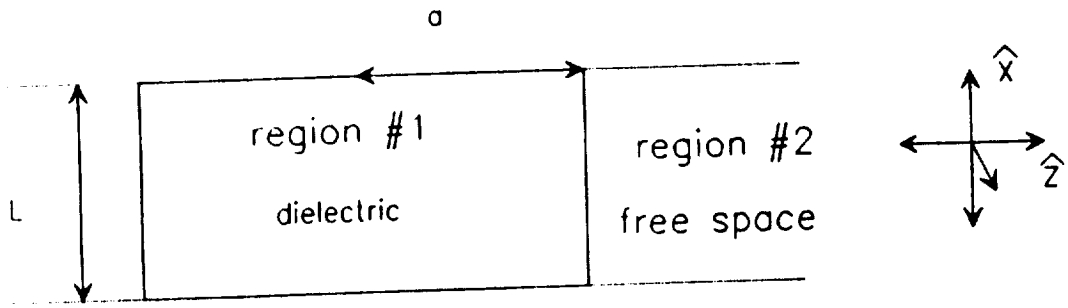

Figure 2.3b Region one and two of the dielectric resonator

The *TE* fields are given by the following relationships [10]:

$$E_\rho = \frac{-1}{\rho}\frac{\partial}{\partial\phi}\Psi^B \qquad (2.7a)$$

$$E_\phi = \frac{\partial}{\partial\rho}\Psi^B \qquad (2.7b)$$

$$E_z = 0 \qquad (2.7c)$$

$$H_\rho = \frac{-1}{j\omega\mu}\frac{\partial^2}{\partial\rho\partial z}\Psi^B \qquad (2.7d)$$

$$H_\phi = \frac{-1}{j\omega\mu\rho}\frac{\partial^2}{\partial\phi\partial z}\Psi^B \qquad (2.7e)$$

$$H_z = \frac{-1}{j\omega\mu}\left(\frac{\partial^2}{\partial z^2} + k_1^2\right)\Psi^B. \qquad (2.7f)$$

In region one, which is the dielectric, the fields must have finite values as ρ approaches zero. To fulfill this criterion the general Bessel function must be an ordinary Bessel function of the 1st kind of order n. The electric fields in the dielectric are found by operating on Eq. 2.3 according to Eq. 2.7 which results in

$$E_\rho^1 = \frac{-jn}{\rho}J_n(k_{1\rho}\rho)\,(C_1\cos(k_z z) + D_1\sin(k_z z))\,e^{jn\phi} \qquad (2.8a)$$

$$E_\phi^1 = k_{1\rho}J_n'(k_{1\rho}\rho)\,(C_1\cos(k_z z) + D_1\sin(k_z z))\,e^{jn\phi} \qquad (2.8b)$$

$$E_z^1 = 0 \qquad (2.8c)$$

$$H_\rho^1 = \frac{-jk_{1\rho}k_z}{\omega_o\mu_o}J_n'(k_{1\rho}\rho)\,(C_1\sin(k_z z) - D_1\cos(k_z z))\,e^{jn\phi} \qquad (2.8d)$$

$$H_\phi^1 = \frac{nk_z}{\omega_o\mu_o\rho}J_n(k_{1\rho}\rho)\,(C_1\sin(k_z z) - D_1\cos(k_z z))\,e^{jn\phi} \qquad (2.8e)$$

$$H_z^1 = \frac{jk_{1\rho}^2}{\omega_o\mu_o}J_n(k_{1\rho}\rho)\,(C_1\cos(k_z z) + D_1\sin(k_z z))\,e^{jn\phi}, \qquad (2.8f)$$

with the prime denoting the derivative with respect to the argument.

In region two, which is free space, all fields must decay to zero as ρ tends towards infinity. Thus, in region two the Bessel function must be a modified Hankel function with an argument of $jk_{2\rho}\rho$. The modified Hankel function with argument $jk_{2\rho}\rho$ represents an outward decaying wave provided that the argument is purely real. The fields in region two are found by

operating on Eq. 2.4 according to Eq. 2.7 which leaves

$$E_\rho^2 = \frac{-jn}{\rho} K_n(jk_{2\rho}\rho)\,(C_2\cos(k_z z) + D_2\sin(k_z z))e^{jn\phi} \tag{2.9a}$$

$$E_\phi^2 = jk_{2\rho} K_n'(jk_{2\rho}\rho)\,(C_2\cos(k_z z) + D_2\sin(k_z z))e^{jn\phi} \tag{2.9b}$$

$$E_z^2 = 0 \tag{2.9c}$$

$$H_\rho^2 = \frac{k_{2\rho}k_z}{\omega_o\mu_o} K_n'(jk_{2\rho}\rho)\,(C_2\sin(k_z z) + D_2\cos(k_z z))e^{jn\phi} \tag{2.9d}$$

$$H_\phi^2 = \frac{nk_z}{\omega_o\mu_o\rho} K_n(jk_{2\rho}\rho)\,(C_2\sin(k_z z) - D_2\cos(k_z z))e^{jn\phi} \tag{2.9e}$$

and

$$H_z^2 = \frac{jk_{2\rho}^2}{\omega_o\mu_o} K_n(jk_{2\rho}\rho)\,(C_2\cos(k_z z) + D_2\sin(k_z z))e^{jn\phi} . \tag{2.9f}$$

The boundary condition as defined by the PMC model, at $\rho = a$, $z = 0$ and $z=h$ are

$$H_\phi^1(\rho = a) = H_\phi^2(\rho = a) = 0, \tag{2.10a}$$

$$H_\phi^1(z = 0) = H_\phi^2(z = 0) = 0, \tag{2.10b}$$

and

$$H_\phi^1(z = h) = H_\phi^2(z = h) = 0. \tag{2.10c}$$

Enforcing boundary condition (2.10a) gives

$$\frac{-nk_z}{\omega_o\mu_o a} J_n(k_{1\rho}a)\,(C_1\cos(k_z z) + D_1\sin(k_z z))\,e^{jn\phi}\,e^{-jk_z z} = 0$$

which simplifies to

$$J_n(k_{1\rho}a) = 0.$$

Define , $x_{nm} = k_{1\rho}$, as the mth root of the Ordinary Bessel function Jn to give a solution

$$k_{1\rho} = \frac{x_{nm}}{a} . \tag{2.11}$$

Enforcing boundary conditions, (2.10b) and (2.10c) give

$$C_1 = 0$$

and

$$D_1 \sin(k_z h) = 0. \tag{2.12}$$

To obtain a non-trivial solution it is required that

$$\sin(k_z h) = 0. \tag{2.13}$$

Eq. 2.13 is satisfied if and only if

$$k_z h = p\pi$$

or

$$k_z = \frac{p\pi}{h} \qquad p = 0, 1, 2, \ldots \tag{2.14}$$

Substituting equations 2.11 and 2.14 into the separation equation (2.5) the resonant frequency is derived as

$$k_1^2 = k_z^2 + k_{1\rho}^2 = \omega_o^2 \mu_o \epsilon_r \epsilon_o$$

$$(2\pi f_r)^2 \mu_o \epsilon_r \epsilon_o = (\frac{p\pi}{h})^2 + (\frac{x_{nm}}{a})^2$$

$$(f_r)_{nmp}^{TE} = \frac{1}{2\pi\sqrt{\mu_o \epsilon_r \epsilon_o}} \sqrt{(\frac{x_{nm}}{a})^2 + (\frac{p\pi}{h})^2} . \tag{2.15}$$

Where the indices n and p may be any non-negative integer and m may be any positive integer. A similar procedure is undertaken to find the resonant frequency of the TM_{nmp} modes (2.16).

$$(f_r)^{TM}_{amp} = \frac{1}{2\pi\sqrt{\mu_o \epsilon_r \epsilon_o}} \sqrt{\left(\frac{x'_{nm}}{a}\right)^2 + \left(\frac{p\pi}{h}\right)^2} \qquad (2.16)$$

The symbol x'_{nm} is the argument for the zero's of the derivatives of the Bessel function and the indices n and p may be non-negative and m any non-negative integer.

The dielectric used in NASA's experiment has a radius of 0.63 cm, a height of 0.51 cm, and a dielectric constant of 40. Using these dimensions, the resonant frequency and propagation constant have been determined for several modes.

mode	f_r (Ghz)	k_z (1/m)
TE_{010}	2.88	0
TE_{110}	4.59	0
TE_{111}	6.53	615
TM_{111}	5.14	615
TM_{011}	6.53	615

2.4 Complete Solution

Before considering the details of the derivation and the approximation that allow for an accurate solution with finite time and resources, insight may be obtained by considering the full scale problem without approximation. The system consists of a lossy dielectric resonator having an excited hybrid mode operating in close proximity to a lossy conductor. Fig. 2.4a illustrates the difficulty. In contrast to an infinite waveguide structure, the dielectric resonator system has a non-separable geometry. The first step of the analysis is to break the system into ten regions as depicted in Figure 2.4b. The Helmholtz's equation is solved in each of the ten regions yielding ten sets of scaler potentials Ψ_{nm}. Then, the fields must be matched at all interfaces. An infinite set of hybrid electro-magnetic fields are found for each region.

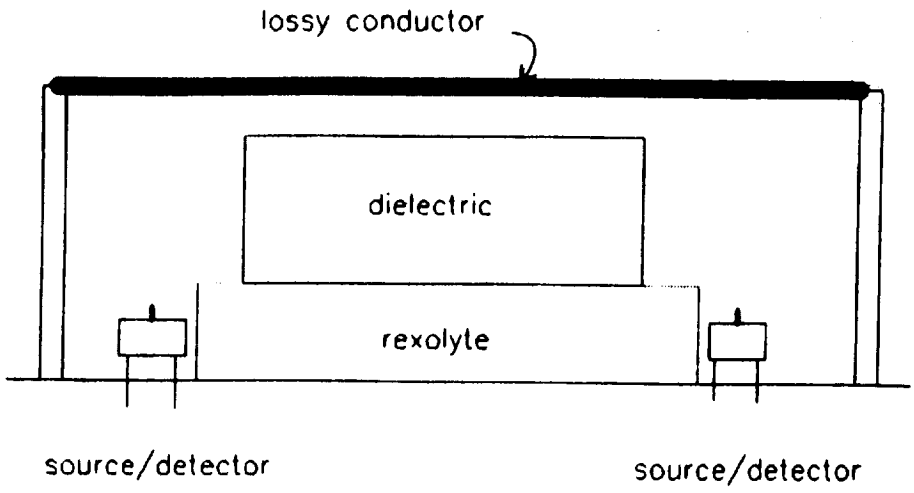

Figure 2.4a Experimental set up

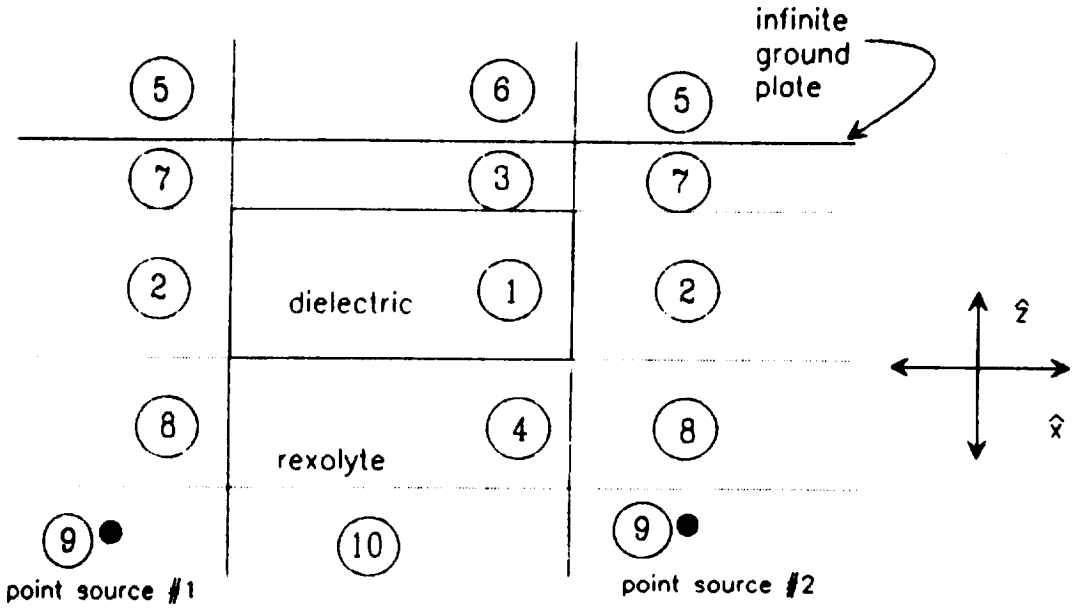

Figure 2.4b Regions of the dielectric resonator

Region one of the dielectric resonator has an infinite number of modes, although only one or a few may dominate. As in the other regions, all but a few of the modes represent evanescent modes. Evanescent modes that radiate into free space represent stored energy and do not effect loss in the system. Evanescent modes that are terminated by a lossy conductor may however have power transfer thus representing a loss mechanism.

To complete the solution, mode-matching techniques are applied at the interface between all regions. The boundary conditions state that the tangential components must be continuous at the region interfaces except at the source interface. As an example, consider region 5.

1) Fields must decay to zero as $z \rightarrow \infty$
2) Fields must decay to zero as $\rho \rightarrow \infty$

and

3) Tangential components must be continuous with the tangential components of region 6 and 7.

The sources may be treated in phase and out of phase to determine the transfer characteristics of the resonator. As an alternate procedure, the complex resonant frequency of a source free region may be determined and the Q of the resonator computed by the ratio of the real to the imaginary frequency terms. The mode-matching procedure outlined above does not guarantee resonance for the source-free problem, rather the procedure must be repeated until a frequency is found for which the fields satisfy all of the equations. This might be stated in terms of the bounce path between the resonator ends providing a gain, with the requirement that the loop gain be of unity magnitude and a net phase change of 0°. The loop gain criteria for resonance will be expanded in Chapter 3. It must be noted that the problem outlined above, although extremely rigorous, is still only an approximation to the real world problem. Two assumptions which delineate this point are the infinite ground plate and the point source. In order to work the problem in a finite amount of time, additional assumptions are necessary.

Each assumption which facilitates easier mathematics must also be justified. In the following development the justification will be that the assumptions deviate slightly from the physical problem and introduce negligible error.

2.5 Outline of the Development

To facilitate a better understanding of the operation of the dielectric resonator system, a five-step "ground-up" development will be employed. The five steps of the development are the analysis of the

1) infinite dielectric rod
2) TE_{01} and TM_{01} resonator
3) HEM_{11} mode resonator
4) dielectric resonator in the presence of a perfect conductor and
5) dielectric resonator in the presence of a lossy conductor.

In step 1 a full field analysis of the infinite dielectric rod (IDR) will yield a method for determining the propagation constant k_z for guided modes. As a result of the derivation, given a complex frequency, radius a, and a complex permittivity ϵ_d, the complex propagation constant may be obtained. Using results of step 1, step 2 derives a formula for the complex reflection coefficient at the resonator's ends. Using the reflection coefficient the criterion for resonance will be forced to yield a complex resonant frequency for the cases of TE_{01} and TM_{01}. Step 3 will use similar techniques of step 2 to determine the complex resonant frequency of a dielectric operating in free space at the lowest order mode hybrid HEM_{11}. Step 4 introduces a perfect conductor to the dielectric system operating with HEM_{11}. In the final step, analysis of a resonator system with a lossy conductor will yield a formula for an equivalent complex reflection coefficient.

Once the complex reflection coefficient is calculated, steps 2-5, the complex resonant frequency of the dielectric resonator can be computed. The method for computing the complex resonant frequency is based on loop gain and phase criteria. Similar to electric oscillator and optical laser cavities requirements for resonance, the loop gain of the system must have a gain of 1 and a change in phase of zero. Specifically for the dielectric resonator, loop gain and phase refer to the electro-magnetic fields, illustrated in Fig. 2.5a. The formula that enforces the criteria of gain and phase is given by

$$\Gamma_{13}\Gamma_{14}\, e^{-j2k_z L} = 1.0 \,. \tag{2.17}$$

A two-dimensional search will be used to determine the complex frequency, S, that minimizes the error of Eq. 2.17. Each complex frequency yields a propagation constant. Given the propagation constant the error function is given by

$$error = |\, 1.0 - \quad \Gamma_{13}\Gamma_{14}\, e^{-j2k_z L}\,| \,. \tag{2.18}$$

The two dimensional search is depicted in Fig. 2.5b. Once the complex frequency, $S = -\zeta + j\omega_o$, is determined, the unloaded qurality factor of the resonant system is given by

$$Q_u = \frac{\omega_o}{\zeta} \,. \tag{2.19}$$

Programs have been written to simulate the operation of the dielectric resonator system with one of three modes exited under different physical conditions. Conditions of special interest are the perturbation of the dielectric loss mechanism ϵ'', the air gap distance between the dielectric and the conductor, and the conductivity of the ground plate. As a result of the work in Chapter 3, given the physical dimensions of the resonator system, the output of the simulation will be the complex propagation constant k_z, complex reflection coefficient, and complex resonant frequency.

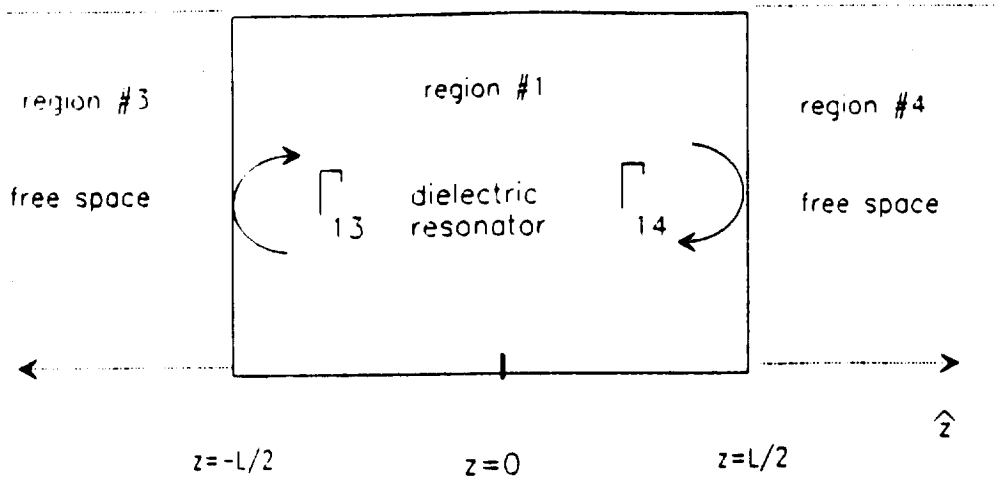

Figure 2.5a Dielectric with reflection coefficients

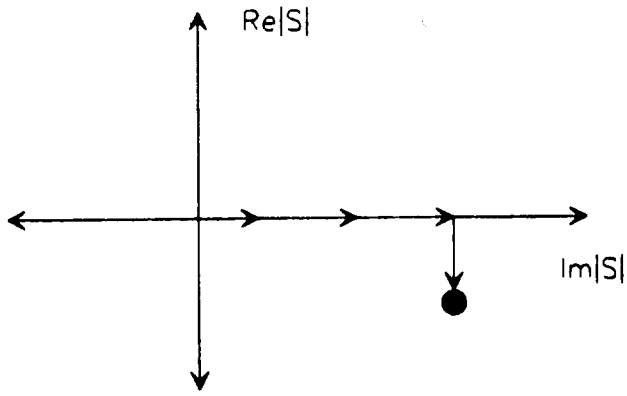

Figure 2.5b Two dimensional search for complex frequency S

Chapter 3

Analytical Development

3.1 Infinite Dielectric Rod

The goals of the first stage of development are two: derive, without approximation, the electro-magnetic fields of the infinite dielectric rod and devise a method for determining the complex propagation constant k_z. The cylindrical dielectric waveguide under consideration is shown in Figure 3.1. Region 1 is the Infinite Dielectric Rod (IDR) and region 2 is the infinite space surrounding the rod. The derivation begins by using two sets of electromagnetic potentials that satisfy Helmholtz's scaler equation in each of the two regions. Restricting the fields to finite values, the electro-magnetic potentials are used to derive the hybrid fields for each of the two regions. Applying the dielectric-dielectric boundary condition, that tangential fields must be continuous across the boundary, results in a system of 4 equations and 5 unknowns. Four of the unknowns are field coefficients, A-D, and the fifth unknown is the propagation constant k_z. The last two tasks of the section will be to develop a method for solving k_z and solving the field coefficients A, B and C relative to coefficient D.

The derivation begins with the magnetic and electric potentials that satisfy Helmholtz's equation in region 1 and 2. These potentials may be written in general form as

$$\Psi^{M}_{1_{nm}} = AB^{m1}_{n}(k_{1\rho}\rho)\, e^{jn\phi}\, e^{-jk_{1z}z} \tag{3.1a}$$

$$\Psi^{E}_{1_{nm}} = BB^{e1}_{n}(k_{1\rho}\rho)\, e^{jn\phi}\, e^{-jk_{1z}z} \tag{3.1b}$$

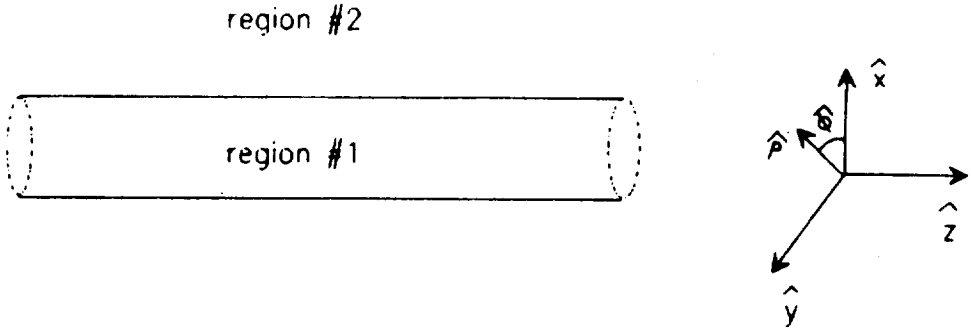

Figure 3.1 Infinite Dielectric Rod

$$\psi^{M}_{2_{nm}} = CB_n^{m2}(k_{2\rho}\rho)\, e^{jn\phi}\, e^{-jk_{2z}z} \tag{3.1c}$$

$$\psi^{E}_{2_{nm}} = DB_n^{e2}(k_{2\rho}\rho)\, e^{jn\phi}\, e^{-jk_{2z}z} \tag{3.1d}$$

The notation B_n^X denotes a general Bessel function of the nth order. The subscript m denotes the mth root of k_ρ solution for a particular n. To be explicit the propagation constant representing mode nm in region 1 would be written $k_{z1_{nm}}$. To satisfy boundary conditions at the dielectric-dielectric interface for all z, it is required that $k_{1z}=k_{2z}$. Thus, the propagation constant will be shortened to k_z.

A direct result of solving the wave equation is the separation equation. The separation equations for the two regions are given by

$$k_1^2 = k_0^2\epsilon_r = k_{1\rho}^2 + k_z^2 = \omega_0^2\mu_0\epsilon_r\epsilon_0 \tag{3.2a}$$

and

$$k_2^2 = k_0^2 = k_{2\rho}^2 + k_z^2 = \omega_0^2\mu_0\epsilon_0 \tag{3.2b}$$

For cylindrical waveguides, modes that exhibit angular variation cannot be pure TE or TM modes. The modes that exhibit angular variation in the cylindrical dielectric are (HEM) hybrid, commonly referred to as either HE or EH modes. HE is used when TE (H) modes are predominant and EH (E) when TM modes are predominant. For dielectric waveguides the dominant mode is HEM_{11} followed by TE_{01}, HEM_{21}, and TM_{01} [10]. TE and TM modes are special cases, n=0, of the infinite hybrid set. Thus, consideration of the hybrid set takes care of all possible modes. The hybrid modes can be written as a superposition of properly operated on potentials ψ^E and ψ^M. The hybrid electric and magnetic fields are given by

$$E_\rho = \frac{1}{j\omega\epsilon}\frac{\partial^2}{\partial\rho\partial z}\psi^M - \frac{1}{\rho}\frac{\partial}{\partial\phi}\psi^E \tag{3.3a}$$

$$H_\rho = \frac{1}{\rho}\frac{\partial}{\partial\phi}\psi^M + \frac{1}{j\omega\mu}\frac{\partial^2}{\partial\rho\partial z}\psi^E \tag{3.3b}$$

$$E_\phi = \frac{1}{j\omega\epsilon\rho}\frac{\partial^2}{\partial\phi\partial z}\Psi^M + \frac{\partial}{\partial\rho}\Psi^E \qquad (3.3c)$$

$$H_\phi = -\frac{\partial}{\partial\rho}\Psi^M + \frac{1}{j\omega\mu\rho}\frac{\partial^2}{\partial\phi\partial z}\Psi^E \qquad (3.3d)$$

$$E_z = \frac{1}{j\omega\epsilon}\left(\frac{\partial^2}{\partial z^2} + k^2\right)\Psi^M \qquad (3.3e)$$

$$H_z = \frac{1}{j\omega\mu}\left(\frac{\partial^2}{\partial z^2} + k^2\right)\Psi^E . \qquad (3.3f)$$

In region 1, the fields must have a finite value as ρ approaches zero. Thus, the general Bessel function is an ordinary Bessel function of the first kind order n. The electric fields in region 1 are thus given as

$$E_\rho^1 = \left[A\frac{-k_{1\rho}k_z}{\omega_o\epsilon_d} J_n'(k_{1\rho}\rho) + B\frac{-jn}{\rho} J_n(k_{1\rho}\rho)\right] e^{jn\phi}e^{-jk_z z} \qquad (3.4a)$$

$$E_\phi^1 = \left[A\frac{-jn\,k_z}{\omega_o\epsilon_d\rho} J_n(k_{1\rho}\rho) + B\,k_{1\rho}J_n'(k_{1\rho}\rho)\right] e^{jn\phi}e^{-jk_z z} \qquad (3.4b)$$

$$E_z^1 = A\frac{-jk_{1\rho}^2}{\omega_o\epsilon_d} J_n(k_{1\rho}\rho)\, e^{jn\phi}e^{-jk_z z} \qquad (3.4c)$$

where $k_{1\rho}^2 = k_1^2 - k_z^2$.

The same method is applied to yield the magnetic field components of region one. Eq. 3.3 operating on 3.1 yield

$$H_\rho^1 = \left[A\frac{jn}{\rho} J_n(k_{1\rho}\rho) + B\frac{-k_{1\rho}k_z}{\omega_o\mu_o} J_n'(k_{1\rho}\rho)\right] e^{jn\phi}e^{-jk_z z} \qquad (3.4d)$$

$$H_\phi^1 = \left[-A\,k_{1\rho}J_n'(k_{1\rho}\rho) + B\frac{-jnk_z}{\omega_o\mu_o\rho} J_n(k_{1\rho}\rho)\right] e^{jn\phi}e^{-jk_z z} \qquad (3.4e)$$

$$H_z^1 = B\frac{-jk_{1\rho}^2}{\omega_o\mu_o} J_n(k_{1\rho}\rho)\, e^{jn\phi}e^{-jk_z z} . \qquad (3.4f)$$

The dielectric of region two is free space with ϵ_o and μ_o and assumed to be infinite in the ρ direction. All fields must be finite as ρ tends toward infinity. This requires the general Bessel function in region 2 to be a modified Hankel function with an argument of $jk_{2\rho}$. The

modified Hankel function with argument $jk_{2\rho}$ represents an outward decaying wave. The field expansions are given as

$$E_\rho^2 = [\, C \frac{-jk_{2\rho}k_{2z}}{\omega_o\epsilon_o} K_n'(jk_{2\rho}\rho) + D \frac{-jn}{\rho} K_n(jk_{2\rho}\rho) \,] e^{jn\phi} e^{-jk_z z} \quad (3.5a)$$

$$E_\phi^2 = [C\frac{-jnk_{2z}}{\omega_o\epsilon_o\rho} K_n(jk_{2\rho}\rho) + D(jk_{2\rho})K_n'(jk_{2\rho}\rho)] e^{jn\phi} e^{-jk_z z} \quad (3.5b)$$

$$E_z^2 = C \frac{-jk_{2\rho}^2}{\omega_o\epsilon_o} K_n(jk_{2\rho}\rho) e^{jn\phi} e^{-jk_z z} \quad (3.5c)$$

where $k_{2\rho}^2 = k_2^2 - k_z^2$. As before, the magnetic field components in region two become

$$H_\rho^2 = [\, C \frac{jn}{\rho} K_n(jk_{2\rho}\rho) + D \frac{-jk_{2\rho}k_{2z}}{\omega_o\mu_o} K_n'(jk_{2\rho}\rho) \,] e^{jn\phi} e^{-jk_z z} \quad (3.5d)$$

$$H_\phi^2 = [\, C(-jk_{2\rho}) K_n'(jk_{2\rho}\rho) + D\frac{-jnk_z}{\omega_o\mu_o\rho} K_n(jk_{2\rho}\rho) \,] e^{jn\phi} e^{-jk_z z} \quad (3.5e)$$

$$H_z^2 = D \frac{-jk_{2\rho}^2}{\omega_o\mu_o} K_n(jk_{2\rho}\rho) e^{jn\phi} e^{-jk_z z} . \quad (3.5f)$$

The fields derived above represent an infinite number of possible field solutions. In addition to the z-dependence, the tangential components must be continuous at the dielectric-dielectric boundary. These boundary conditions may be written as

$$1)\ H_z^1(\rho=a,\ 0 \le \phi \le 2\pi,\ z) = H_z^2(\rho=a,\ 0 \le \phi \le 2\pi,\ z) \quad (3.6a)$$

$$2)\ E_z^1(\rho=a,\ 0 \le \phi \le 2\pi,\ z) = E_z^2(\rho=a,\ 0 \le \phi \le 2\pi,\ z) \quad (3.6b)$$

$$3)\ H_\phi^1(\rho=a,\ 0 \le \phi \le 2\pi,\ z) = H_\phi^2(\rho=a,\ 0 \le \phi \le 2\pi,\ z) \quad (3.6c)$$

and

$$4)\ E_\phi^1(\rho=a,\ 0 \le \phi \le 2\pi,\ z) = E_\phi^2(\rho=a,\ 0 \le \phi \le 2\pi,\ z). \quad (3.6d)$$

Substituting the field expansions into the boundary conditions, we obtain the following four equations:

$$B\,k_{1\rho}^2\;J_n(k_{1\rho}a) = D\,k_{2\rho}^2\;K_n(jk_{2\rho}a) \tag{3.7a}$$

$$A\;k_{1\rho}^2\;J_n(k_{1\rho}a) = C\epsilon_r\,k_{2\rho}^2\;K_n(jk_{2\rho}a) \tag{3.7b}$$

$$A\,k_{1\rho}J'_n(k_{1\rho}a) + B\frac{jnk_1}{\omega_o\mu_o a}\,J_n(k_{1\rho}a) = C\,jk_{2\rho}K'_n(jk_{2\rho}a) + D\frac{jnk_1}{\omega_o\mu_o a}\,K_n(jk_{2\rho}a) \tag{3.7c}$$

and

$$A\,\frac{-jn\,k_1}{\omega_o\epsilon_d a}\,J_n(k_{1\rho}a) + B\,k_{1\rho}J'_n(k_{1\rho}a) = C\,\frac{-jn\,k_1}{\omega_o\epsilon_o a}\;K_n(jk_{2\rho}a) + D\,jk_{2\rho}K'_n(jk_{2\rho}a). \tag{3.7d}$$

These four equations can be set equal to zero and written in matrix form

$$Z_{nm}x=0. \tag{3.8}$$

The quantity x is the eigenvector of the coefficients given by

$$x = \begin{bmatrix} A \\ B \\ C \\ D \end{bmatrix} \tag{3.9}$$

and matrix Z_{nm} is given by

$$Z_{nm} = \begin{bmatrix} 0 & k_{1\rho}^2 J_n(k_{1\rho}a) & 0 & -k_{2\rho}^2 K_n(jk_{2\rho}a) \\ k_{1\rho}^2 J_n(k_{1\rho}a) & 0 & -\epsilon_r k_{2\rho}^2 K_n(jk_{2\rho}a) & 0 \\ k_{1\rho} J_n'(k_{1\rho}a) & \frac{jnk_z}{\omega_o \mu_o a} J_n(k_{1\rho}a) & -jk_{2\rho} K_n'(jk_{2\rho}a) & \frac{-jnk_z}{\omega_o \mu_o a} K_n(jk_{2\rho}a) \\ \frac{-jnk_z}{\omega_o \epsilon_d a} J_n(k_{1\rho}a) & k_{1\rho} J_n'(k_{1\rho}a) & \frac{jnk_z}{\omega_o \epsilon_o a} K_n(jk_{2\rho}a) & -jk_{2\rho} K_n'(jk_{2\rho}a) \end{bmatrix}$$

where the matrix elements are a function of k_z. The k_ρ component for regions one and two are given by

$$k_{1\rho_{nm}} = \sqrt{\omega^2 \mu_o \epsilon_o \epsilon_r - k_{z_{nm}}^2} \tag{3.10a}$$

and

$$k_{2\rho_{nm}} = \sqrt{\omega^2 \mu_o \epsilon_o - k_{z_{nm}}^2} \tag{3.10b}$$

The subscripts *nm* are added to emphasize that there are multiple solutions corresponding to the nth harmonic in ϕ and mth root of the matrix equation. There are two possible solution forms for eigensystem (3.8). The first trivial possibility is that the eigenvector is equal to zero. The second possibility is a solution requiring the determinant of Z equal to zero. Since 3.8 is a function of k_z, to have a non-trivial solution there must exist a particular k_z that forces the determinant of Z to zero. The technique used to find the particular complex propagation constant k_z is outlined below.

A direct search algorithm is used to find the k_z root by first searching the dominant phase term for a minimum determinant and setting

$$k_z = j\beta_{min}.$$

The method used to find β searches starting with β_0, increments by $\Delta\beta$, and ends at β_1 where

$$\beta_0 = \sqrt{\omega_0^2 \mu_0 \epsilon_0}$$

and

$$\beta_1 = \sqrt{\omega_0^2 \mu_0 \epsilon_0 \epsilon_r}.$$

Any β outside this specified range will be imaginary, representing an evanescent wave. As β is incremented, the magnitude of the determinant Z_{nm}, denoted by $|Z_{nm}|$, is calculated to determine which β yields the minimum determinant magnitude. The results of this method is shown in Fig. 3.2 for

$$freq = 9.54\ Ghz$$

$$a = 0.635\ cm$$

and

$$\epsilon_r = 40 - j0.04.$$

Once β_{min} has been established, k_z is set equal to $k_z = \beta_{min}$ and a second search is undertaken to find the real part of the complex propagation constant. The real part of k_z is incremented in search of the particular k_z that minimizes $|Z_{nm}|$ (Fig. 3.2b). Once the two dimensional search is completed the propagation constant is given by

$$k_z = \beta_{min} - j\alpha_{min}. \tag{3.11}$$

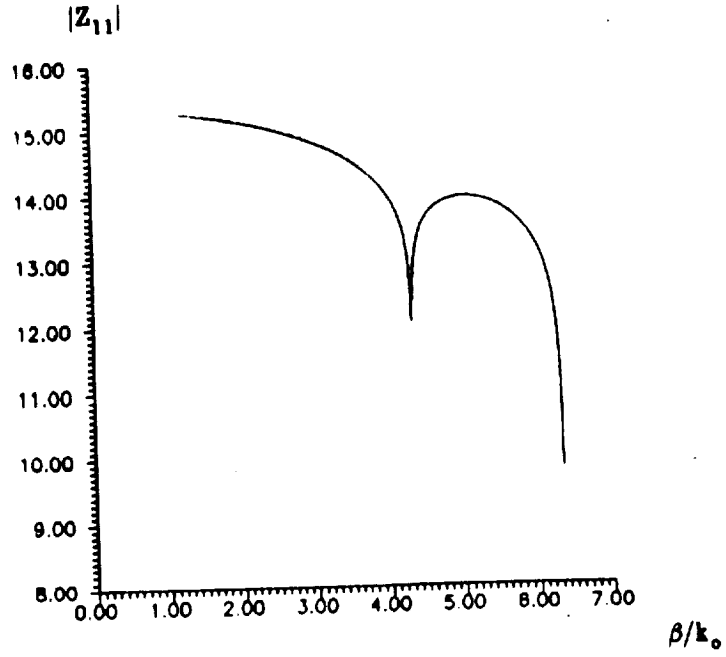

Figure 3.2a Determinant magnitude vs. β/k_o

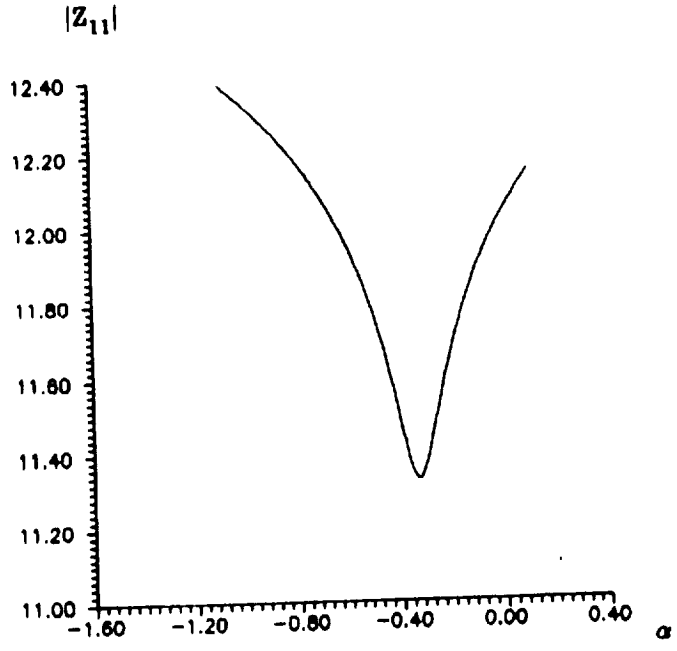

Figure 3.2b Determinant magnitude vs. α for $\beta = 4.3 \cdot k_o$

The results of the two dimensional search for this example provides the solution

$k_z = 319.0 - j0.336$ for the HEM_{11} mode.

The negative imaginary component implies attenuation of the forward propagating waves. Having computed the propagation constant k_z, the ρ component can be determined using Equation 3.10. The ρ components are

$k_{1\rho} = 344.0 - j0.00837$

$k_{2\rho} = -0.345 - j0.336.$

Once k_z is computed, it is insightful to determine the coefficients A, B, and C relative to D. The coefficients are related to the magnitude of the field components and can be determined to within a constant without having information about the source. With knowledge of the source, a Green's function technique may be used to determine the four coefficients. For the purpose of this paper, it is sufficient to calculate the coefficients A, B, and C relative to coefficient D.

To determine the relative coefficients, matrix system (3.8) is written in the form

$$\begin{bmatrix} 0 & f_{12} & 0 & f_{14} \\ f_{21} & 0 & f_{23} & 0 \\ f_{31} & f_{32} & f_{33} & f_{34} \\ f_{41} & f_{42} & f_{43} & f_{44} \end{bmatrix} \begin{bmatrix} A \\ B \\ C \\ D \end{bmatrix} = \begin{bmatrix} 0 \\ 0 \\ 0 \\ 0 \end{bmatrix}, \qquad (3.12)$$

which has the form

$Zx = 0.$

Taking the LU decomposition of Z leaves the matrix in the form

$$\begin{bmatrix} \hat{f}_{11} & \hat{f}_{12} & \hat{f}_{13} & \hat{f}_{14} \\ 0 & \hat{f}_{22} & \hat{f}_{23} & \hat{f}_{24} \\ 0 & 0 & \hat{f}_{33} & \hat{f}_{34} \\ 0 & 0 & 0 & \hat{f}_{44} \end{bmatrix} \begin{bmatrix} A \\ B \\ C \\ D \end{bmatrix} = \begin{bmatrix} 0 \\ 0 \\ 0 \\ 0 \end{bmatrix} \tag{3.13}$$

The last equation of the matrix system is

$$D\Delta\hat{f}_{44} = 0\,, \tag{3.14}$$

where $\Delta\hat{f}_{44} \approx 0$. Eq. 3.14 allows D to be assigned any value. The simple choice of D = 1 may be used to obtain a 3x3 matrix in the form of

$$\tilde{Z}\,\tilde{x} = g, \tag{3.15}$$

$$\begin{bmatrix} \hat{f}_{11} & \hat{f}_{12} & \hat{f}_{13} \\ 0 & \hat{f}_{22} & \hat{f}_{23} \\ 0 & 0 & \hat{f}_{33} \end{bmatrix} \begin{bmatrix} A \\ B \\ C \end{bmatrix} = \begin{bmatrix} -\hat{f}_{14} \\ -\hat{f}_{24} \\ -\hat{f}_{34} \end{bmatrix} \tag{3.16}$$

where g is a constant, and the vector $\tilde{x}$ may found to yield A, B, C relative to D. Coding all the

work outlined above allows the field components of equations 3.4 and 3.5 to be plotted versus ρ. Using the dimensions and properties of the NASA experiment, the 6 field components versus ρ are plotted in Fig. 3.3 for the HEM_{11} mode. So that the electric and magnetic field strengths can be compared, the fields are given in units of $\frac{V}{m}$. Several observations can be made to intuitively check the results including

1) tightly bound fields

2) continuity of tangential fields

3) discontinuity of the E_ρ components by a factor of ϵ_r.

4) predominately TE (no E_z)

The field pattern for HEM_{11} is shown in Figure 3.4. The knowledge of the field configuration for the specific dimension of the experiment is essential in the further development of the dielectric resonator system.

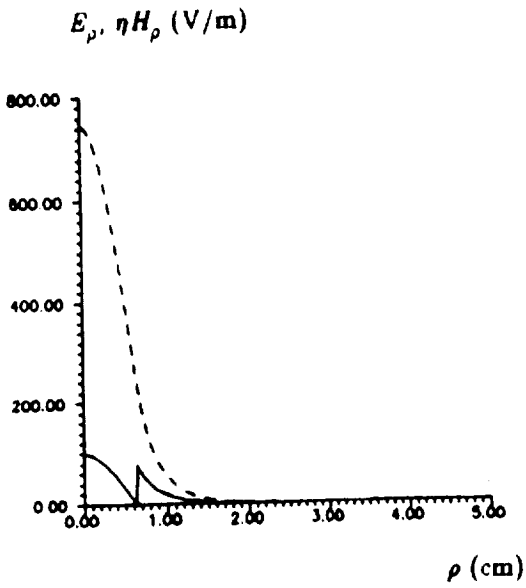

Figure 3.3a $E_\rho, \eta H_\rho$(---) vs. ρ

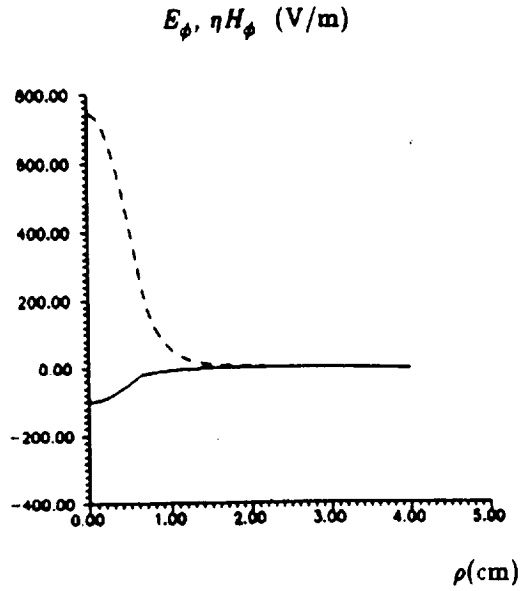

Figure 3.3b $E_\phi, \eta H_\phi$(---) vs. ρ

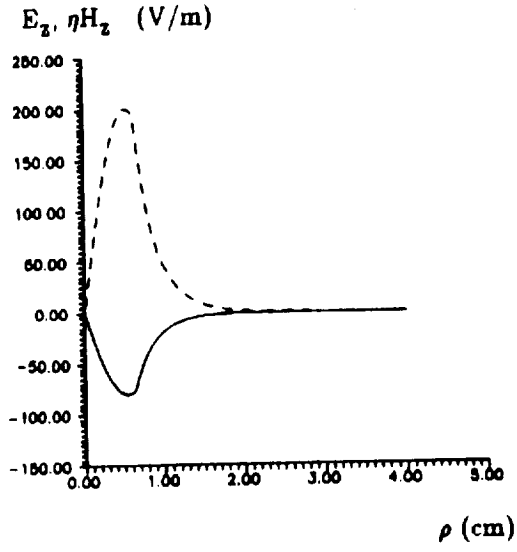

Figure 3.3c $E_z, \eta H_z$(---) vs. ρ

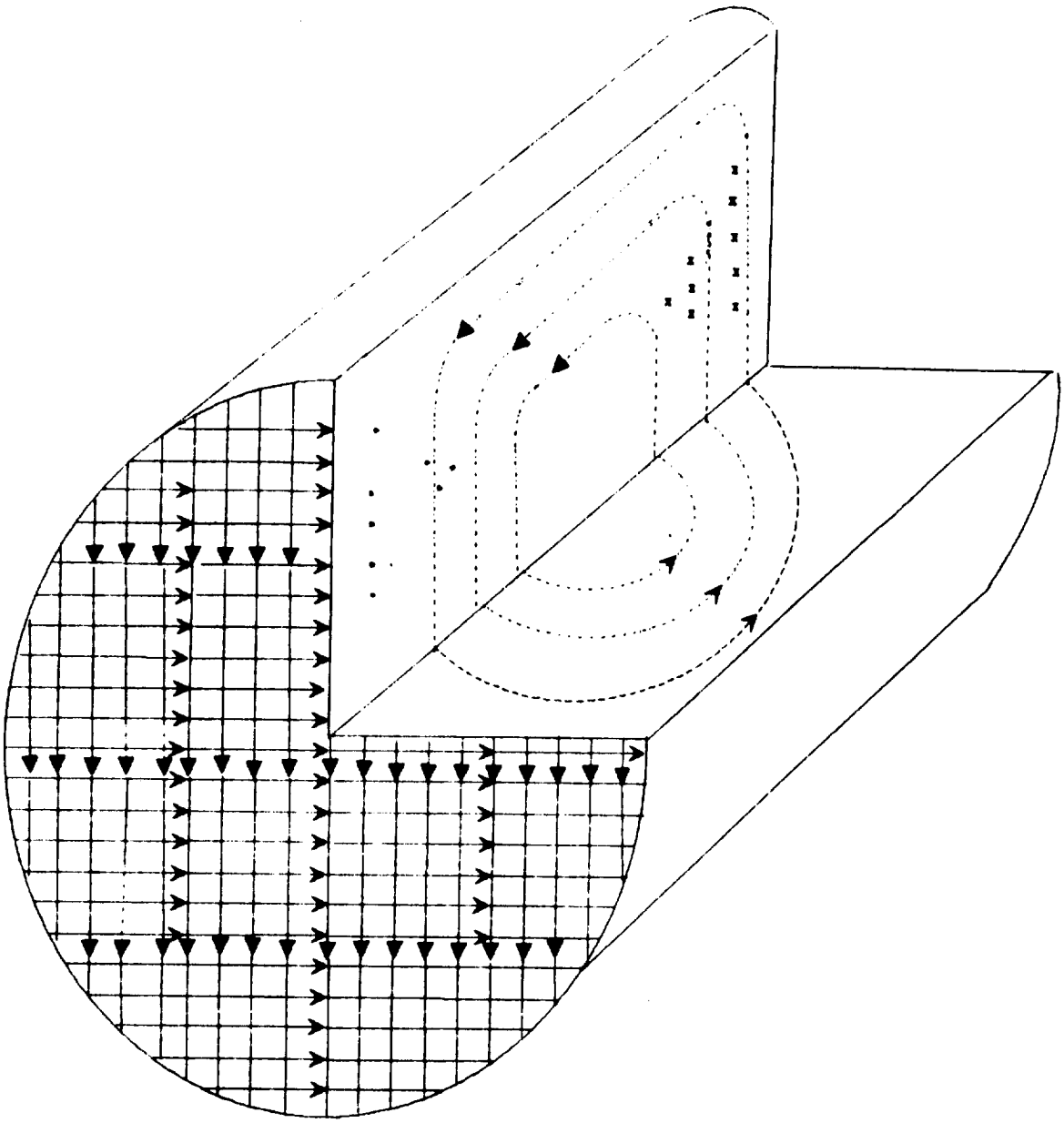

Figure 3.4 Field distribution of hybrid mode HEM_{11}
(E——,H- - -)

3.2 Resonator Method for TE_{01}

As stated in Section 2.2, the mode that is dominant depends on the physical dimensions and properties of the dielectric. In addition, the experimental setup, such as the orientation of the probes, plays an essential role in determining which modes are excited. One of the possible low order modes that may be dominant is the TE_{01} mode. In this section, the complex reflection coefficient will be derived for a free space dielectric resonator (Fig. 3.5) having a single dominant TE_{01} field configuration as in Section 2.2.

By considering both forward and reflected waves at the resonator end, $z = \frac{L}{2}$, the expression for the reflection coefficient, Γ_{13}, may be formulated. As outlined in Section 2.6, the reflection coefficient will be used to iteratively solve for the dielectric's complex resonant frequency. The derivation begins by using the results from the infinite dielectric rod of Section 3.1. The zeroth order electro-magnetic fields are obtained by setting n = 0. In addition, A and C are set equal to zero which results in pure transverse electric waves. The TE_{01} fields in region one are given by

$$E_\phi^1 = Bk_{1\rho} J_0'(k_{1\rho}\rho) e^{-jk_z z} \tag{3.17a}$$

$$H_\rho^1 = B\frac{-k_{1\rho}k_z}{\omega_o\mu_o} J_0'(k_{1\rho}\rho) e^{-jk_z z} \tag{3.17b}$$

$$H_z^1 = B\frac{-jk_{1\rho}^2}{\omega_o\mu_o} J_0(k_{1\rho}\rho) e^{-jk_z z} \tag{3.17c}$$

and in region two by

$$E_\phi^2 = Djk_{2\rho} K_0'(jk_{2\rho}\rho) e^{-jk_z z} \tag{3.18a}$$

$$H_\rho^2 = D\frac{-jk_{2\rho}k_z}{\omega_o\mu_o} K_0'(jk_{2\rho}\rho) e^{-jk_z z} \tag{3.18b}$$

$$H_z^2 = D\frac{-jk_{2\rho}^2}{\omega_o\mu_o} K_0(jk_{2\rho}\rho) e^{-jk_z z} . \tag{3.18c}$$

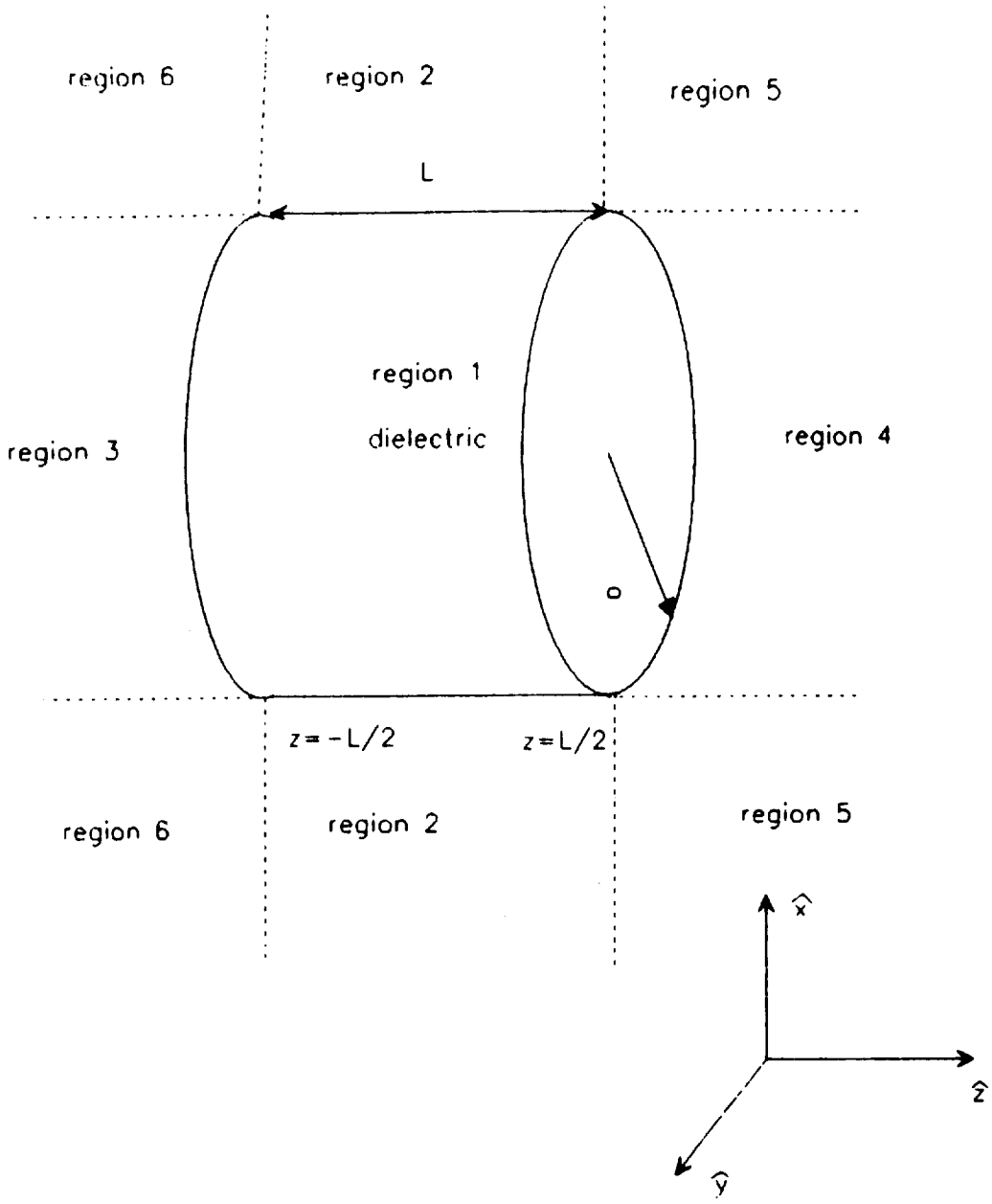

Figure 3.5 Post dielectric resonator

Along the dielectric-air interface, ρ=a, the tangential components from region one to region two must be continuous. These two boundary conditions are stated in by Eq. 3.19a and 3.19b.

$$1)\ E_{\phi}^{1}(\rho=a) = E_{\phi}^{2}(\rho=a) \tag{3.19a}$$

$$2)\ H_{z}^{1}(\rho=a) = H_{z}^{2}(\rho=a) \tag{3.19b}$$

Dividing (3.19b) by (3.19a) results in

$$\frac{k_{1\rho}J_0(k_{1\rho}a)}{J_0'(k_{1\rho}a)} + \frac{jk_{2\rho}K_0(jk_{2\rho}a)}{K_0'(jk_{2\rho}a)} = 0$$

or

$$k_{1\rho}J_0(k_{1\rho}a)\,K_0'(jk_{2\rho}a) + jk_{2\rho}K_0(jk_{2\rho}a)J_0'(k_{1\rho}a) = 0. \tag{3.20}$$

It should be noted that Eq. 3.20 is a special case of the eigensystem (3.8). If the matrix approach is used, setting n=0 would result in two possible solutions corresponding to TE_{0m} and TM_{0m}. Satisfying Eq. 3.20 is an infinite set of eigenvalues $k_{z_{0m}}$ with the subscript m taking on values of 1 to infinity. The corresponding $k_{\rho_{0m}}$ components can be found from

$$k_{1\rho_{0m}} = \sqrt{(\omega_o^2\mu_o\epsilon_d - k_{z_{0m}}^2)} \tag{3.21a}$$

and

$$k_{2\rho_{0m}} = \sqrt{(\omega_o^2\mu_o\epsilon_o - k_{z_{0m}}^2)}\,. \tag{3.21b}$$

From this point, only the first solution, m=1, will be considered and the subscript m=1 will be implicit. The development proceeds by matching field components at the end of the resonator shown in Fig. 3.6. At interface, $z=\frac{L}{2}$, the tangential components of region one must equal the tangential components of region four. The fields in region one are composed of a forward and reflected traveling waves. The reflected waves are given by substituting $k_z = -k_z$ into equation 3.17. In region four it is assumed that the fields have the same k_ρ component as

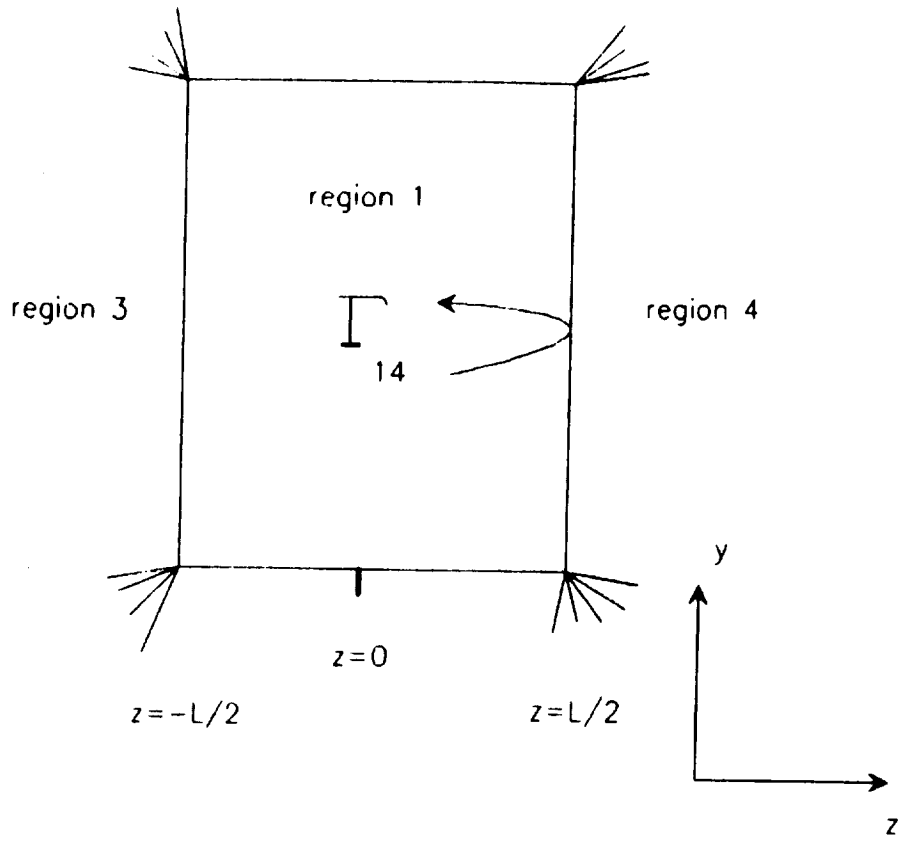

z=L/2

Figure 3.6 Reflection Coefficient at interface z=L/2

the fields in region one. This assumption in effect ignores the fringe fields, depicted in Fig. 3.6, of the resonator. The error associated with this assumption will be small if the fringe area is small compared to the total surface area of the resonator end and the evanescent fields decay rapidly in the z direction. It follows that if $k_{4\rho} = k_{1\rho}$ in region four, the propagation constant k_{4z} is obtained from

$$k_{4z} = -\sqrt{\omega_o^2 \mu_o \epsilon_o - k_{1\rho}^2} \tag{3.22}$$

The negative imaginary root is chosen to give decay as z goes to infinity. The boundary condition for the TE_{01} mode at the end interface is given by

$$1)\ E_\phi^{1^+}(z=\tfrac{L}{2}) + E_\phi^{1^-}(z=\tfrac{L}{2}) = E_\phi^4(z=\tfrac{L}{2}) \tag{3.23a}$$

and

$$2)\ H_\rho^{1^+}(z=\tfrac{L}{2}) + H_\rho^{1^-}(z=\tfrac{L}{2}) = H_\rho^4(z=\tfrac{L}{2}) . \tag{3.23b}$$

The corresponding reflection coefficient Γ_{14} is defined at $z = \frac{L}{2}$ as

$$\Gamma_{14} = \frac{E_1^-}{E_1^+} = \frac{-H_1^-}{H_1^+} . \tag{3.24}$$

Using z = 0 as a phase reference Eq. 3.23 can be rewritten using Eq. 3.24 which yields

$$E_\phi^{1^+}(1+\Gamma_{14}) = E_\phi^4 \tag{3.25a}$$

and

$$H_\rho^{1^+}(1-\Gamma_{14}) = H_\phi^4 \tag{3.25b}$$

Using $z=\frac{L}{2}$ as the phase reference, the field components are

$$E_{\phi}^{1+} = Bk_{1\rho} J'_0(k_{1\rho}\rho)\, e^{-jk_z(z-\frac{L}{2})} \tag{3.26a}$$

$$E_{\phi}^{4} = B_4 k_{1\rho} J'_0(k_{1\rho}\rho)\, e^{-jk_{4z}(z-\frac{L}{2})} \tag{3.26b}$$

$$H_{\rho}^{1+} = B\frac{-k_{1\rho}k_z}{\omega_0\mu_0} J'_0(k_{1\rho}\rho)\, e^{-jk_z(z-\frac{L}{2})} \tag{3.26c}$$

and

$$H_{\phi}^{4} = B_4\frac{-k_{1\rho}k_{4z}}{\omega_0\mu_0} J'_0(k_{1\rho}\rho)\, e^{-jk_{4z}(z-\frac{L}{2})}. \tag{3.26d}$$

The boundary conditions (3.25a) can be rewritten as

$$Bk_{1\rho} J'_0(k_{1\rho}\rho)(1+\Gamma_{14}) = B_4 k_{1\rho} J'_0(k_{1\rho}\rho)$$

$$B(1+\Gamma_{14}) = B_4. \tag{3.27}$$

Boundary condition 3.25b can be rewritten as

$$B\frac{-k_{1\rho}k_z}{\omega_0\mu_0} J'_0(k_{1\rho}\rho)\,(1-\Gamma_{14}) = B_4\frac{-k_{1\rho}k_{4z}}{\omega_0\mu_0} J'_0(k_{1\rho}\rho)$$

$$k_z B(1-\Gamma_{14}) = B_4 k_{4z} \tag{3.28}$$

Dividing 3.27 by 3.28 yields

$$\frac{1+\Gamma_{14}}{k_z(1-\Gamma_{14})} = \frac{1}{k_{4z}}$$

$$\Gamma_{14} = \frac{k_z - k_{4z}}{k_z + k_{4z}} \qquad (TE_{01}) \tag{3.29}$$

The reflection coefficient for a single dominant TM_{01} can be derived using Eq. 3.4 and setting n, B and D equal to zero. Proceeding in similar manner, as for the reflection coefficient for transverse electric, the transverse magnetic reflection coefficient is

$$\Gamma_{14} = \frac{\epsilon_r k_{4z} - k_{4z}}{\epsilon_r k_z + k_z} \qquad (TM_{01}). \tag{3.30}$$

Having derived the complex reflection coefficient allows the algorithm developed in Section 2.6 to be implemented and yields the complex resonant frequency. Shown below is the result of the gain/phase criterion agrees with Itoh's method [4]. The resonator has a dielectric constant $\epsilon_r = 40 - j0.04$ (loss tangent 0.001), a radius of 0.63 cm and a height L of 0.51 cm.

mode	method	k_z	S $(\alpha+j\omega_o)$ Hz
TE_{011}	PMC	615.7	$-2{,}737{,}800 + j2\pi \cdot 5.476\text{x}10^9$
TE_{011}	Itoh	354.672 – j0.353	$-2{,}200{,}000 + j2\pi \cdot 4.375\text{x}10^9$
TE_{011}	Phase/Gain	354.670 – j0.351	$-2{,}200{,}000 + j2\pi \cdot 4.375\text{x}10^9$

As shown in this section, computing the complex resonant frequency for the dielectric resonator mode TE_{01} can be done using Gain/Phase criterion. Confidence and validity of the Gain/Phase method is given by concurrence with Itoh's method, which is theoretically equivalent. In the next section, attention is turned to the problem of computing the resonant frequency for hybrid modes.

3.3 Hybrid Resonator

As mentioned in Section 3.1 the lowest order mode for a cylindrical dielectric waveguide is the hybrid HEM_{11} mode. Other nomenclature used to describe the lowest order mode is HE_{11} which denotes that the mode is dominantly transverse electric. In this section, the problems associated with solving for the complex reflection coefficient for hybrid modes are outlined. Several approaches addressing these problems are presented. The problem for this specific resonator is resolved by applying the insight gained in the development of the infinite dielectric waveguide in Section 3.1 to the dielectric resonator.

The task of formulating a closed-form solution for the reflection coefficient, as derived for the TE and TM cases, will prove to be formidable. In fact, it will be shown that using a mode-matching technique, as employed for the TE and TM cases, will lead to a numeric ambiguity of four equations and three unknowns. Several approaches are considered to resolve this problem. The final approach will draw from information obtained in the study of the infinite dielectric waveguide in Section 3.1, and the field distribution unique to the physical dimensions and material parameters of the experiment under study.

The derivation begins by matching the forward and reflected waves of region one (Fig. 3.7) to the fields of region four. The boundary condition equalities may be written as

$$E_\rho^{1+} + E_\rho^{1-} = E_\rho^4 \tag{3.31a}$$

$$E_\phi^{1+} + E_\phi^{1-} = E_\phi^4 \tag{3.31b}$$

$$H_\rho^{1+} + H_\rho^{1-} = H_\rho^4 \tag{3.31c}$$

$$H_\phi^{1+} + H_\phi^{1-} = E_\phi^4 \tag{3.31d}$$

As in Section 3.2, the fringe fields are ignored and a tightly bounded field configuration is assumed. The propagation constant in region four is

$$k_{4z} = \sqrt{\omega_o^2 \mu_o \epsilon_o - k_{1\rho}^2} \,. \tag{3.32}$$

Using the electromagnetic fields of Eq. 3.4 and noting that the reflected waves have propagation constant $-k_z$, the boundary conditions may be rewritten as

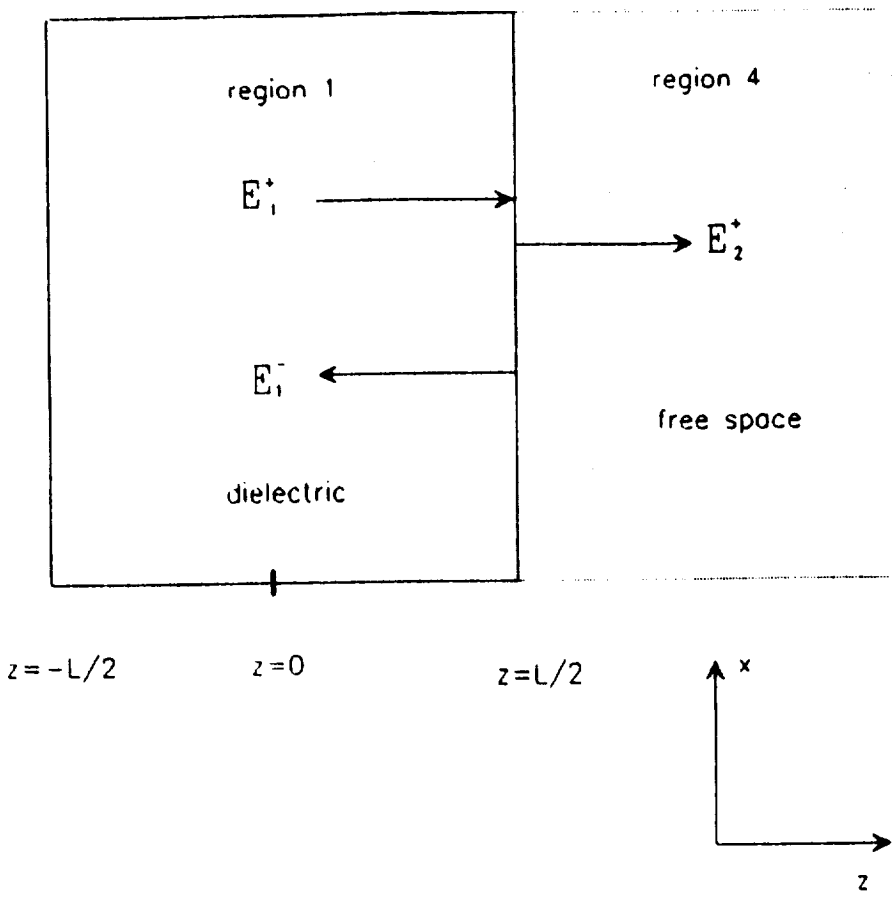

Figure 3.7 Incedent, reflected and transmitted wave

$$(A\frac{k_{1\rho}k_z}{\omega_o\epsilon_d}J'_n(k_{1\rho}\rho)+B\frac{jn}{\rho}J_n(k_{1\rho}\rho))(e^{-jk_z\frac{L}{2}}+\Gamma_{14}e^{jk_z\frac{L}{2}})=$$

$$(A_4\frac{k_{1\rho}k_{4z}}{\omega_o\epsilon_o}J'_n(k_{1\rho}\rho)+B_4\frac{-jn}{\rho}J_n(k_{1\rho}\rho))e^{-jk_{4z}\frac{L}{2}} \quad (3.33a)$$

$$(A\frac{-jnk_z}{\omega_o\epsilon_d\rho}J_n(k_{1\rho}\rho)+Bk_{1\rho}J'_n(k_{1\rho}\rho))(e^{-jk_z\frac{L}{2}}+\Gamma_{14}e^{jk_z\frac{L}{2}})=$$

$$(A_4\frac{-jnk_{4z}}{\omega_o\epsilon_o\rho}J_n(k_{1\rho}\rho)+B_4k_{1\rho}J'_n(k_{1\rho}\rho))e^{-jk_{4z}\frac{L}{2}} \quad (3.33b)$$

$$(A\frac{jn}{\rho}J_n(k_{1\rho}\rho)+B\frac{-k_{1\rho}k_z}{\omega_o\mu_o}J'_n(k_{1\rho}\rho))(e^{-jk_z\frac{L}{2}}-\Gamma_{14}e^{jk_z\frac{L}{2}})=$$

$$(A_4\frac{jn}{\rho}J_n(k_{1\rho}\rho)+B_4\frac{-k_{1\rho}k_{4z}}{\omega_o\mu_o}J'_n(k_{1\rho}\rho))e^{-jk_{4z}\frac{L}{2}} \quad (3.33c)$$

and

$$(-Ak_{1\rho}J'_n(k_{1\rho}\rho)+B\frac{-jnk_z}{\omega_o\mu_o\rho}J_n(k_{1\rho}\rho))(e^{-jk_z\frac{L}{2}}-\Gamma_{14}e^{jk_z\frac{L}{2}})=$$

$$(-A_4k_{1\rho}J'_n(k_{1\rho}\rho)+B_4\frac{-jnk_{4z}}{\omega_o\mu_o\rho}J_n(k_{1\rho}\rho))e^{-jk_{4z}\frac{L}{2}} \quad (3.33d)$$

Using the numeric methods developed in Section 3.1, the coefficients A, B, C, and D can be found relative to D for the forward and reflected waves. Knowing the propagation constant k_{4z} and the four coefficients, A, B, C and D leaves the four equations with the three unknowns Γ_{14}, A_4, B_4. Rearranging equation 3.33 such that the unknowns are on the left of the equality leaves

$$-\Gamma_{14}(A\frac{k_{1\rho}k_z}{\omega_o\epsilon_d}J'_n(k_{1\rho}\rho)+B\frac{jn}{\rho}J_n(k_{1\rho}\rho))e^{jk_z\frac{L}{2}}+A_4(\frac{k_{1\rho}k_{4z}}{\omega_o\epsilon_o}J'_n(k_{1\rho}\rho)e^{-jk_{4z}\frac{L}{2}})$$

$$+B_4(\frac{jn}{\rho}J_n(k_{1\rho}\rho)e^{-jk_{4z}\frac{L}{2}})=(A\frac{k_{1\rho}k_z}{\omega_o\epsilon_d}J'_n(k_{1\rho}\rho)+B\frac{jn}{\rho}J_n(k_{1\rho}\rho))e^{-jk_z\frac{L}{2}} \quad (3.34a)$$

$$-\Gamma_{14}(A\frac{-jnk_z}{\omega_o\epsilon_d\rho}J_n(k_{1\rho}\rho)+Bk_{1\rho}J'_n(k_{1\rho}\rho))e^{jk_z\frac{L}{2}}+A_4(\frac{-jnk_{4z}}{\omega_o\epsilon_o\rho}J_n(k_{1\rho}\rho)e^{-jk_{4z}\frac{L}{2}})$$

$$+B_4(k_{1\rho}J_n'(k_{1\rho}\rho)e^{-jk_{4z}\frac{L_t}{2}}) = (A\frac{-jnk_z}{\omega_o\epsilon_d\rho}J_n(k_{1\rho}\rho) + Bk_{1\rho}J_n'(k_{1\rho}\rho))e^{-jk_z\frac{L_t}{2}} \quad (3.34b)$$

$$\Gamma_{14}(A\frac{jn}{\rho}J_n(k_{1\rho}\rho) + B\frac{-k_{1\rho}k_z}{\omega_o\mu_o}J_n'(k_{1\rho}\rho))e^{jk_z\frac{L_t}{2}}) + A_4(\frac{jn}{\rho}J_n(k_{1\rho}\rho)e^{-jk_{4z}\frac{L_t}{2}})$$

$$+ B_4(\frac{-k_{1\rho}k_{4z}}{\omega_o\mu_o}J_n'(k_{1\rho}\rho))e^{-jk_{4z}\frac{L_t}{2}}) = (A\frac{jn}{\rho}J_n(k_{1\rho}\rho) + B\frac{-k_{1\rho}k_z}{\omega_o\mu_o}J_n'(k_{1\rho}\rho))e^{-jk_z\frac{L_t}{2}} \quad (3.34c)$$

and

$$\Gamma_{14}(-Ak_{1\rho}J_n'(k_{1\rho}\rho) + B\frac{-jnk_z}{\omega_o\mu_o\rho}J_n(k_{1\rho}\rho))e^{jk_z\frac{L_t}{2}}) + A_4(k_{1\rho}J_n'(k_{1\rho}\rho)e^{-jk_{4z}\frac{L_t}{2}})$$

$$+ B_4\frac{-jnk_{4z}}{\omega_o\mu_o\rho}J_n(k_{1\rho}\rho))e^{-jk_{4z}\frac{L_t}{2}} = (-Ak_{1\rho}J_n'(k_{1\rho}\rho) + B\frac{-jnk_z}{\omega_o\mu_o\rho}J_n(k_{1\rho}\rho))e^{-jk_z\frac{L_t}{2}} \quad (3.34d)$$

Each of the constants is assigned a function designator to indicate the position such as

$$f_{11}(\rho) = (A\frac{k_{1\rho}k_z}{\omega_o\epsilon_d}J_n'(k_{1\rho}\rho) + B\frac{jn}{\rho}J_n(k_{1\rho}\rho))e^{jk_z\frac{L_t}{2}}.$$

This allows for 3.34 to be written in the matrix form

$$\begin{bmatrix} f_{11}(\rho) & f_{12}(\rho) & f_{13}(\rho) \\ f_{22}(\rho) & f_{22}(\rho) & f_{23}(\rho) \\ f_{31}(\rho) & f_{32}(\rho) & f_{33}(\rho) \\ f_{41}(\rho) & f_{42}(\rho) & f_{43}(\rho) \end{bmatrix} \begin{bmatrix} \Gamma_{14} \\ A_3 \\ B_3 \end{bmatrix} = \begin{bmatrix} g_1(\rho) \\ g_2(\rho) \\ g_3(\rho) \\ g_4(\rho) \end{bmatrix} \quad (3.35)$$

which is in the form of

$$Z(\rho)\,u = G(\rho). \quad (3.36)$$

Several problems must be addressed. First, the problem is over specified by having one more equation than unknown. Second, the 4x3 system is a function of ρ. A decision must be made where at the resonator ends to match the fields. The restrictions of the choice are $0 \leq \rho \leq a$, where ρ is the variable that must be chosen and a is the radius of the resonator. One approach is to rank the four boundary equations (3.31) in order of their importance and the least important equation could be "thrown out". The information obtained from the infinite dielectric waveguide could be used to make a judicious decision. A second approach using all four equations employs a more elegant method of a weighted integration over the radius.

In this method the first step is to forward multiply the system of (3.36) by its own transpose. This step may be written as

$$Z^{t}(\rho) \cdot Z(\rho)\, u = Z^{t}(\rho) \cdot G(\rho). \tag{3.37}$$

As a result of the multiplication the 4x3 matrix $Z(\rho)$ of (3.36) becomes a 3x3 system (3.37). Next, to resolve the problem of which point ρ to pick along the radius, the equation may be integrated along ρ leaving

$$\int_0^a [w(\rho) Z^{t}(\rho) \cdot Z(\rho)\, u]\, d\rho = \int_0^a w(\rho) Z^{t}(\rho) \cdot G(\rho)\, d\rho \tag{3.38}$$

The function $w(\rho)$ is a weighting factor that is chosen to facilitate the integration. A judicious choice of $w(\rho)$ could yield a reasonable closed form solution of (3.38). More realistically, numeric integration techniques would be applied to solve for the vector u. Integrating and realizing a solution is beyond the scope of this work.

An alternate approach uses the insight gained from the earlier study of the infinite dielectric waveguide of Section 3.1. Fig. 3.3 shows that the transverse electric field components of the HEM_{11} dominate the components in the direction of propagation. Thus, in this approach the calculation of the complex reflection coefficient will be done by assuming HEM_{nm} boundary

conditions along the resonator, $\rho = a$, and TE_{nm} boundary conditions at the resonators ends. The reflection coefficient for the TE case derived in Section 3.2 is

$$\Gamma_{14} = \frac{k_z - k_{4z}}{k_z + k_{4z}} . \tag{3.39}$$

Implementing the algorithm developed in Chapter 2 using Eq. 3.39 yields Figure 3.8. The graphs show the first two resonant frequencies of HEM_{11}. The first two resonant frequencies are designated f_{111} and f_{112}. The properties and dimensions of the dielectric resonator are

$\epsilon_r = 40 - j0.04$

$a = 0.63$ cm

and

$L = 0.51$ cm,

yielding the complex resonant frequency

$$S = -1.2 \cdot 10^7 + j2\pi \cdot 3.535 \cdot 10^9 \quad (HEM_{11}),$$

field parameters

$f_{r_{111}} = 3.54\ Ghz$

$k_0 = 74.15 + j0.04\ m^{-1}$

$k_{1\rho} = 344.15 + j0.044\ m^{-1}$

$k_{2\rho} = -0.03 - j309.86\ m^{-1}$

$k_z = 318.6 - j0.02\ m^{-1}$

$k_{3z} = -0.036 + j336.07\ m^{-1}$

and

$\Gamma_{14} = -5.42 \cdot 10^{-2} - j0.9977.$

The second order resonant frequency $f_{r_{112}}$ is

$$S = -1.2 \cdot 10^7 + j2\pi \cdot 6.44 \cdot 10^9 \quad (HEM_{11}).$$

From Fig. 3.9a-d it is evident that a percentage of the fields are external to the dielectric. These evanescent fields in free space represent stored energy. From examination of Fig. 3.9, it can be determined that the external fields approach zero as ρ approaches 2 cm. Fig. 3.9d displays how the fields decay at the resonators ends for a resonator in free space, suggesting the importance of the external fields is of paramount importance to the experiment under study. External fields must be understood in order to couple energy effectively into the system from the probes, not perturb the experiment with the experimental support structures, and perturb the fields in a repeatable way with the different conductors. Section 3.4 exams the effect of bringing a perfect conductor within close proximity to the resonators end. From Fig. 3.9d it can be seen that close proximity is within 0.5 cm.

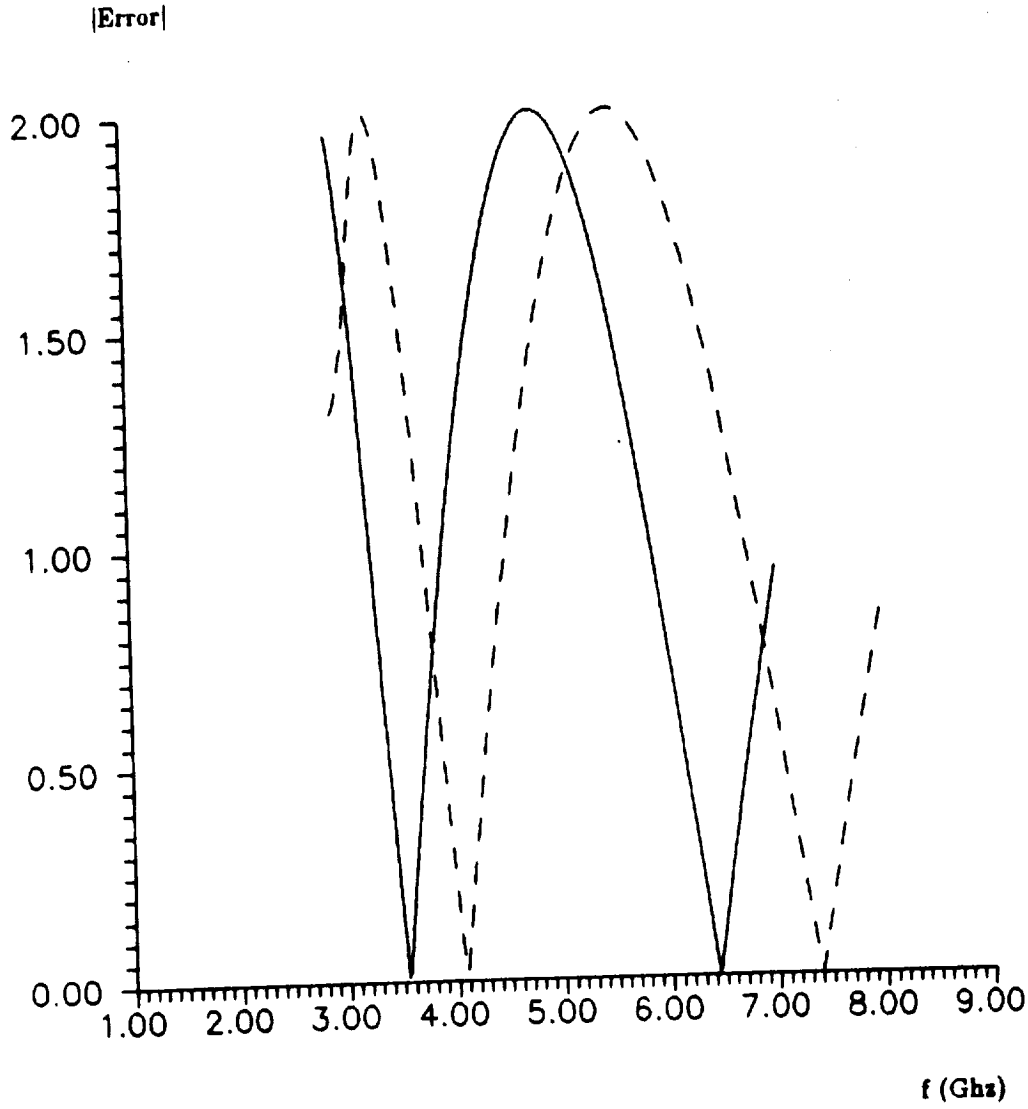

Figure 3.8 Error vs. frequency, the minimums are solutions $f_{r_{111}}$ and $f_{r_{112}}$ ($\epsilon_r = 40$ ---, $\epsilon_r = 30$ - - -)

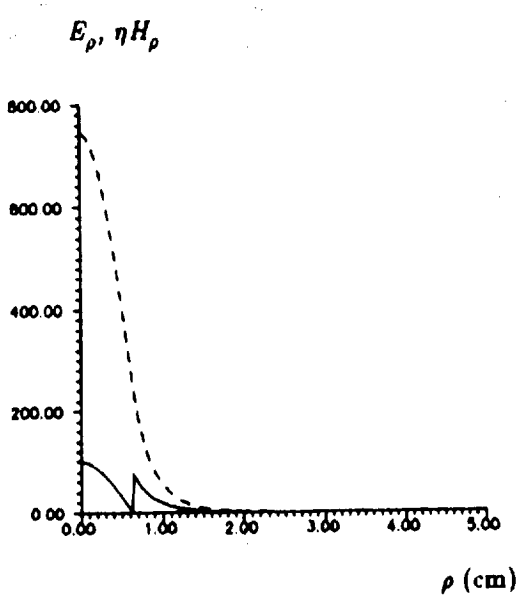

Figure 3.9a $E_\rho, \eta H_\rho$(---) vs. ρ

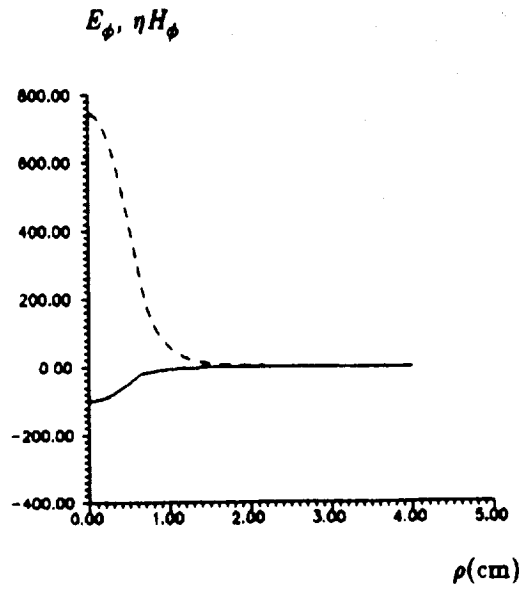

Figure 3.9b $E_\phi, \eta H_\phi$(---) vs. ρ

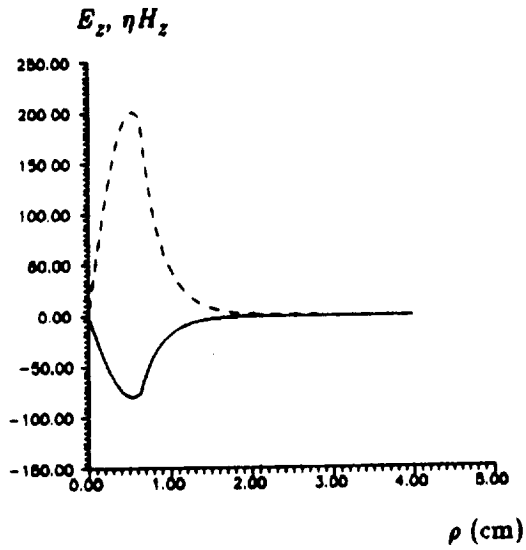

Figure 3.9c $E_z, \eta H_z$(---) vs. ρ

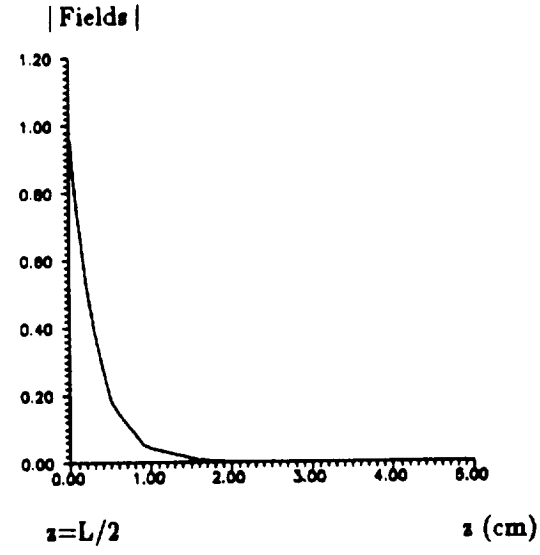

Figure 3.9d Fields vs. z

3.4 Dielectric in the Presence of a Perfect Conductor

This section focuses on the dielectric resonator in the presence of a perfect ground plate as depicted in Figure 3.10a. It is the goal of this section to derive a method of computing the complex resonant frequency as a function of the distance between the dielectric and the perfect conductor. The distance between dielectric and conductor will be referred to as Δz. Before deriving an expression for the reflection coefficient, it is useful to anticipate the results that the derivation will yield

1) as $\Delta z \rightarrow \infty$ $\Gamma_{14} = \Gamma_{13}$ (Γ_{13} – free space resonator)

and

2) as $\Delta z \rightarrow 0$ $|\Gamma_{14}| = 1$ (perfect conductor pressed against dielectric).

The first statement indicates that when the perfect ground-plate is placed infinitely far from the dielectric, the reflection coefficient Γ_{14}, becomes that of free space and yields the same resonant frequencies as those in Section 3.3. The second statement describes perfect reflection as the lossless ground-plate is pressed against the dielectric resonator. In the second case the dielectric pressed against the conductor should yield the same resonant frequency with the same transverse field distribution as a dielectric in free space with a length 2L (Fig. 3.10b). That resonant frequency for the free space resonant dielectric with length 2L will be the hybrid mode HEM_{112}.

The derivation for the reflection coefficient begins by considering the electric potential in region 4

$$\Psi_4^e = J_0(k_{1\rho}\rho)[A_4 \cos(k_{4z}(z+\tfrac{L}{2}+\Delta z)) + B_4 \sin(k_{4z}(z+\tfrac{L}{2}+\Delta z))] . \tag{3.40}$$

Once again the fringe fields are ignored and it is assumed that the k_ρ's are equal in regions one and four. Thus k_{4z} can be given by

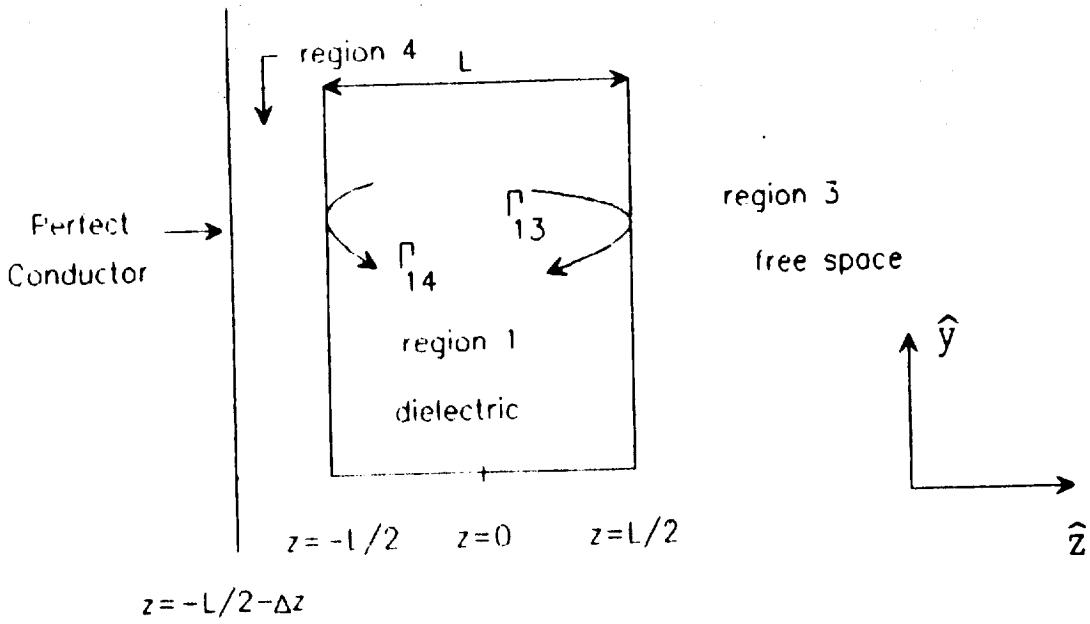

Figure 3.10a Dielectric resonator in close proximity to a perfect dielectric

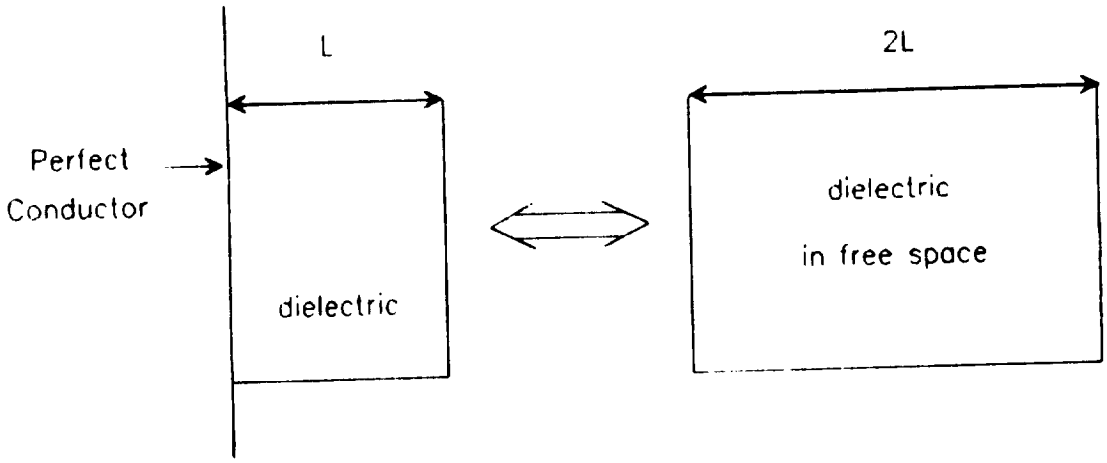

Figure 3.10b Configurations yield equivalent resonate frequency and transverse field distribution

$$k_{4z} = +\sqrt{\omega_o^2 \mu_o \epsilon_o - k_{1\rho}^2} \quad . \tag{3.41}$$

The positive root is chosen to give decay in the -z direction. The ϕ component of the electric field is given by

$$E_\phi^4 = \frac{\partial}{\partial \rho} \Psi_4^e = k_{1\rho} J_0'(k_{1\rho}\rho)[A_4 \cos(k_{4z}(z+\tfrac{L}{2}+\Delta z)) + B_4 \sin(k_{4z}(z+\tfrac{L}{2}+\Delta z))] .$$

At the air-conductor interface, $z = -(\frac{L}{2}+\Delta z)$,

$$E_\phi^4 = k_{1\rho} J_0'(k_{1\rho}\rho)[A_4 \cos(k_{4z}(0)) + B_4 \sin(k_{4z}(0))] = 0$$

or

$$A_4 = 0 .$$

Using this result, the potential Ψ_4^e, and Eq. 3.3, the TE_{01} fields for region four are given by

$$E_\phi^4 = B_4 k_{1\rho} J_0'(k_{1\rho}\rho) \sin(k_{4z}(z+\tfrac{L}{2}+\Delta z)) \tag{3.42a}$$

$$H_\rho^4 = B_4 \frac{-jk_{1\rho}k_{4z}}{\omega_o \mu_o} J_0'(k_{1\rho}\rho) \cos(k_{4z}(z+\tfrac{L}{2}+\Delta z)) \tag{3.42b}$$

$$H_z^4 = B_4 \frac{-j k_{1\rho}^2}{\omega_o \mu_o} J_0(k_{1\rho}\rho) \sin(k_{4z}(z+\tfrac{L}{2}+\Delta z)) . \tag{3.42c}$$

Using $z = \frac{-L}{2}$ as a phase reference, the H_ρ's and E_ϕ's in region one at $z = \frac{-L}{2}$ are

$$E_\phi^{1-} = B k_{1\rho} J_0'(k_{1\rho}\rho) \tag{3.43a}$$

$$E_\phi^{1+} = \Gamma_{14} B k_{1\rho} J_0'(k_{1\rho}\rho) \tag{3.43b}$$

$$H_\rho^{1-} = B \frac{k_{1\rho}k_z}{\omega_o \mu_o} J_0'(k_{1\rho}\rho) \tag{3.43c}$$

$$H_\rho^{1+} = -\Gamma_{14} B \frac{k_{1\rho}k_z}{\omega_o \mu_o} J_0'(k_{1\rho}\rho) . \tag{3.43d}$$

where the reflection coefficient is defined as

$$\Gamma_{14} = \frac{E_\phi^{1-}}{E_\phi^{1+}} = \frac{-H_\rho^{1-}}{H_\rho^{1+}} \quad . \tag{3.44}$$

At the air-dielectric interface, $z = \frac{L}{2}$, the boundary conditions are

$$E_\phi^{1+} + E_\phi^{1-} = E_\phi^4 \tag{3.45a}$$

and

$$H_\rho^{1+} + H_\rho^{1-} = H_\rho^4 . \tag{3.45b}$$

Substituting (3.43) , (3.44) and (3.42) and into the boundary equations yields

$$B\,(\Gamma_{14} + 1) = B_4 \sin(k_{4z}\Delta z) \tag{3.46}$$

and

$$Bk_z\,(-\Gamma_{14} + 1) = -jB_4 k_{4z} \cos(k_{4z}\Delta z) \tag{3.47}$$

Dividing (3.46) by (3.47) and solving for the reflection coefficient gives

$$\Gamma_{14} = \frac{k_z \tan(k_{4z}\Delta z) - jk_{4z}}{k_z \tan(k_{4z}\Delta z) + jk_{4z}} \quad . \tag{3.48}$$

As Δz approaches zero, the reflection coefficient becomes

$$\lim_{\Delta z \to 0} \Gamma_{14} = \frac{+jk_{4z}}{-jk_{4z}} = -1 \ .$$

Providing that Eq. 3.41 yields an imaginary k_{4z}, as the perfect conductor is moved an infinite distance from the dielectric the reflection coefficient is

$$\lim_{\Delta z \to \infty} \Gamma_{14} = \frac{k_z(-j) + j\,k_{4z}}{k_z(-j) - jk_{4z}} = \frac{k_z - k_{4z}}{k_z + k_{4z}} \quad .$$

As $\Delta z \to \infty$ the reflection coefficient becomes identical to that of the free space resonator in section 3.2. Having solved for Γ_{14} in terms of Δz allows the plotting of complex resonant frequency of the first two HEM_{11} modes vs. Δz as shown in Fig. 3.11 and Fig. 4.12 respectively.

In the final stage of development Section 3.5 considers the dielectric resonator in the presence of a lossy conductor.

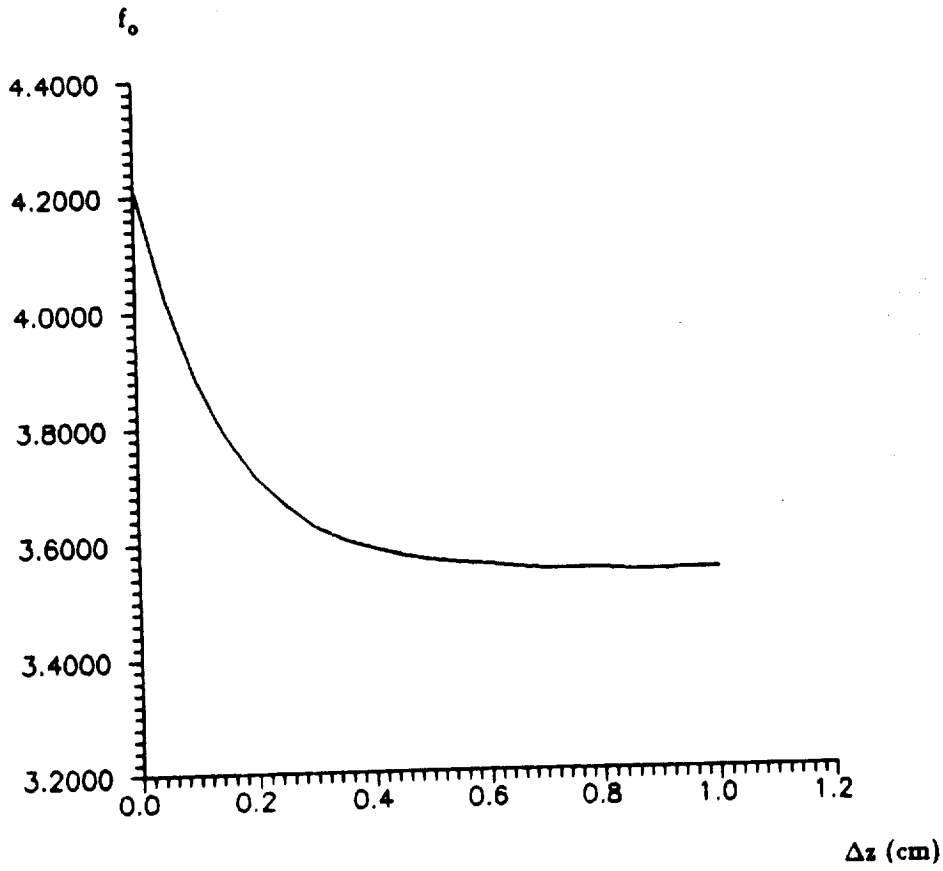

Figure 3.11 Perfect conductor at Δz from dielectric for f_{111}

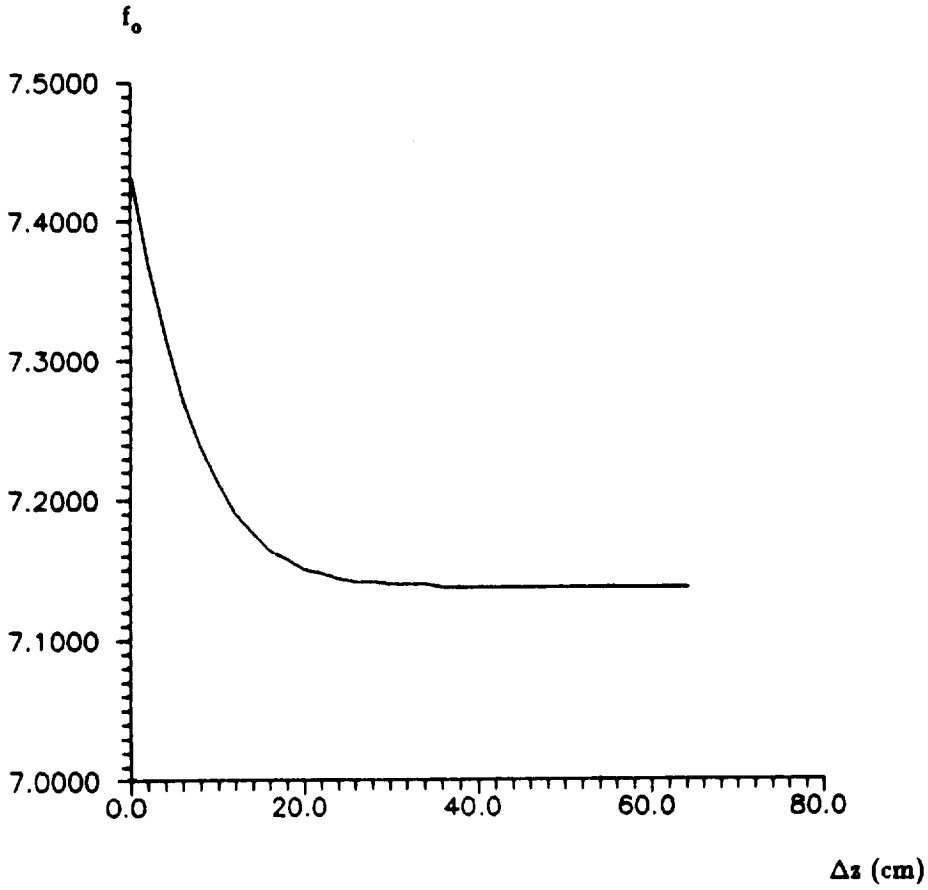

Figure 3.12 Perfect conductor at Δz from dielectric for f_{112}

3.5 Dielectric in the Presence of a Lossy Conductor

The development in this last section is the essence of the thesis: the post dielectric resonator operating in the presence of a lossy conductor. This section will develop and implement the mathematical tools that map the change of the resonant frequency due to the change in the conductivity of the conductor. The objective requires the derivation of an equivalent reflection coefficient that incorporates the air gap and the lossy conductor (Fig. 3.13a). To derive an expression for Γ_{eq}, transmission line theory is employed. The equivalent transmission line problem is shown in Fig. 3.13b. The voltage source is terminated into a transmission line of characteristic impedance z_1 and length a. Section one of the transmission line terminates into a line with characteristic impedance z_2 at length b, which in turn is terminated into load Z_l.

To formulate a solution for the equivalent reflection coefficient, Γ_{eq}, multiple reflections must be accounted for. The two reflection coefficients are

Γ_{14} – reflection from the dielectric-air boundary

and

Γ_{dlc} – reflection form the air-lossy conductor boundary.

First, it should be noted, Γ_{14} and Γ_{dlc} are functions of a single interface. For example, Γ_{14} , developed in Section 3.4, is unique and specific to the dielectric-air interface. Second, Γ_{dlc} is unique and specific to the air-conductor interface. To further complicate the problem there are an infinite number of reflections in the air gap, or in Section 2 of the analogous transmission line. The equivalent reflection coefficient must take in to account each of the reflections mentioned above.

Field theory can solve the problem by using an infinite series to solve for the reflections of the air gap. A more convenient approach employs a technique used in control theory.

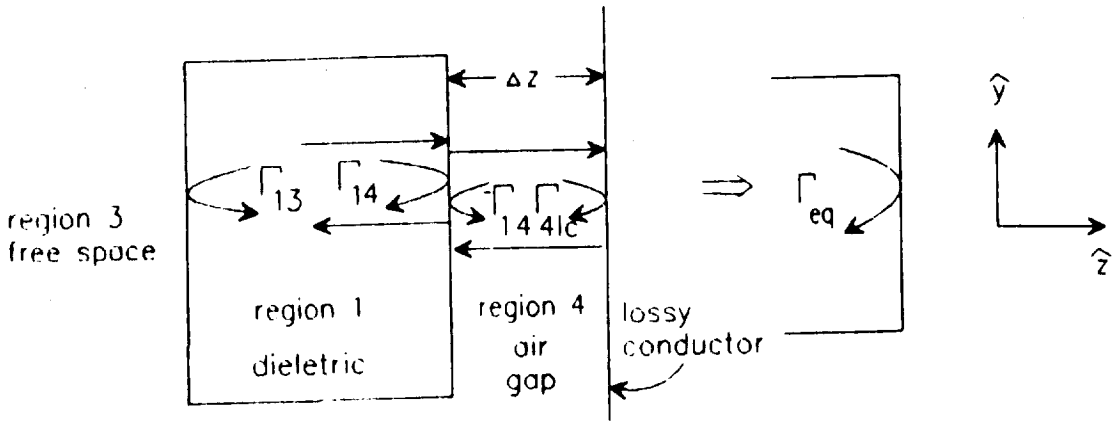

Figure 3.13a Resonator system and equivalent

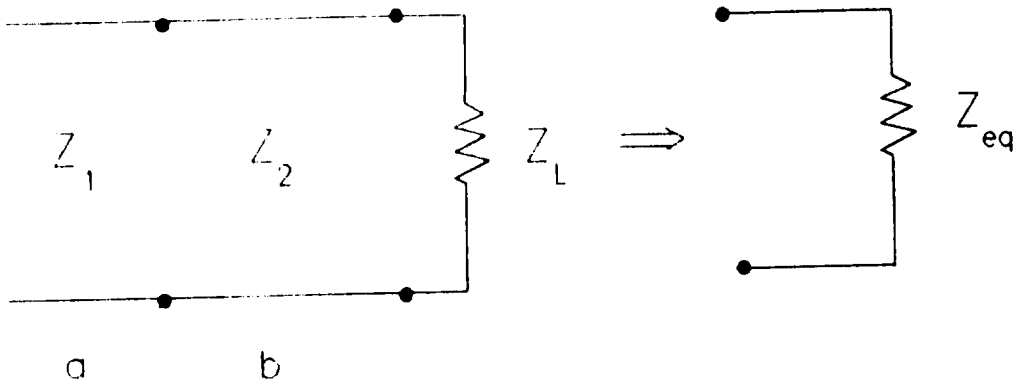

Figure 3.13b Transmission line and equivalent

Treating the air gap as a feedback mechanism, the equivalent reflection coefficient may be written as

$$\Gamma_{eq} = \Gamma_{14} + \frac{(1+\Gamma_{14})(1+\Gamma_{14})\Gamma_{4lc}\, e^{-j2k_{4z}\Delta z}}{1+\Gamma_{14}\Gamma_{4lc}\, e^{-j2k_{4z}\Delta z}} \tag{3.49}$$

Which reduces 3.50 to

$$\Gamma_{eq} = \frac{\Gamma_{14}+\Gamma_{4lc}\, e^{-j2k_{4z}\Delta z}}{1+\Gamma_{14}\Gamma_{4lc}\, e^{-j2k_{4z}\Delta z}} \tag{3.50}$$

The reflection coefficient Γ_{14}, developed in Section 3.3 is

$$\Gamma_{14} = \frac{k_3 - k_{4z}}{k_z + k_{4z}} \tag{3.51}$$

The reflection coefficient for the air-conductor boundary is

$$\Gamma_{4lc} = \frac{k_{4z} - k_{cz}}{k_{4z} + k_{cz}} \tag{3.52}$$

where k_{4z} is

$$k_{4z} = \pm\sqrt{\omega^2\mu_0\epsilon_0 - k_{1\rho}^2}.$$

Care must be taken in the choosing of the proper root. The negative sign is chosen to give decay to fields propagating in the positive *z* direction.

As in Section 3.2, the fringe fields are ignored and tightly bounded fields are assumed. It will also be assumed that the *rho* components of the electric field in the air, lossy conductor, and dielectric are equal. The lossy conductor is assumed to be a good conductor having the

properties [14]

$$\frac{\sigma}{\omega_o \epsilon} > 1000$$

and

$$k_{cs} \simeq \sqrt{\frac{\omega_o \mu_o \sigma}{2}} + j\sqrt{\frac{\omega_o \mu_o \sigma}{2}} \,. \tag{3.53}$$

Using the newly developed propagation constant and equivalent reflection coefficient, the complex resonant frequency can be calculated for the conductor at different conductivities. Fig. 3.14 and 3.15 are the result of using the following parameters

$\epsilon_r = 40 - j0.04$

$\Delta z = 0.2$ cm

$a = 0.635$ cm

and

$h = 0.51$ cm.

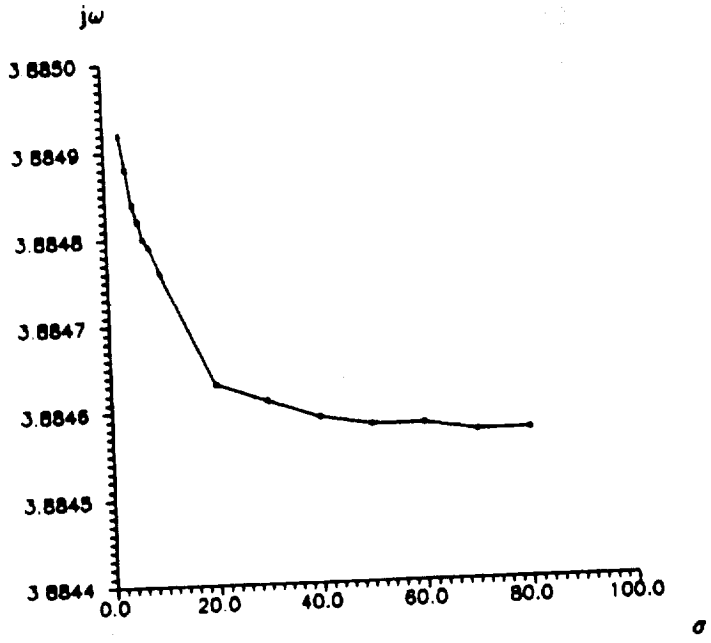

Figure 3.15a Im |S| as a function of conductivity

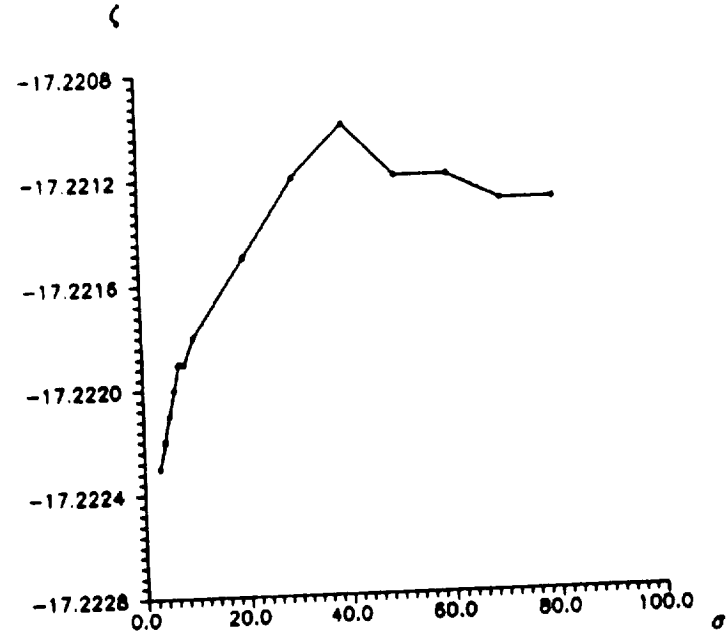

Figure 3.15b Re |S| as a function of conductivity

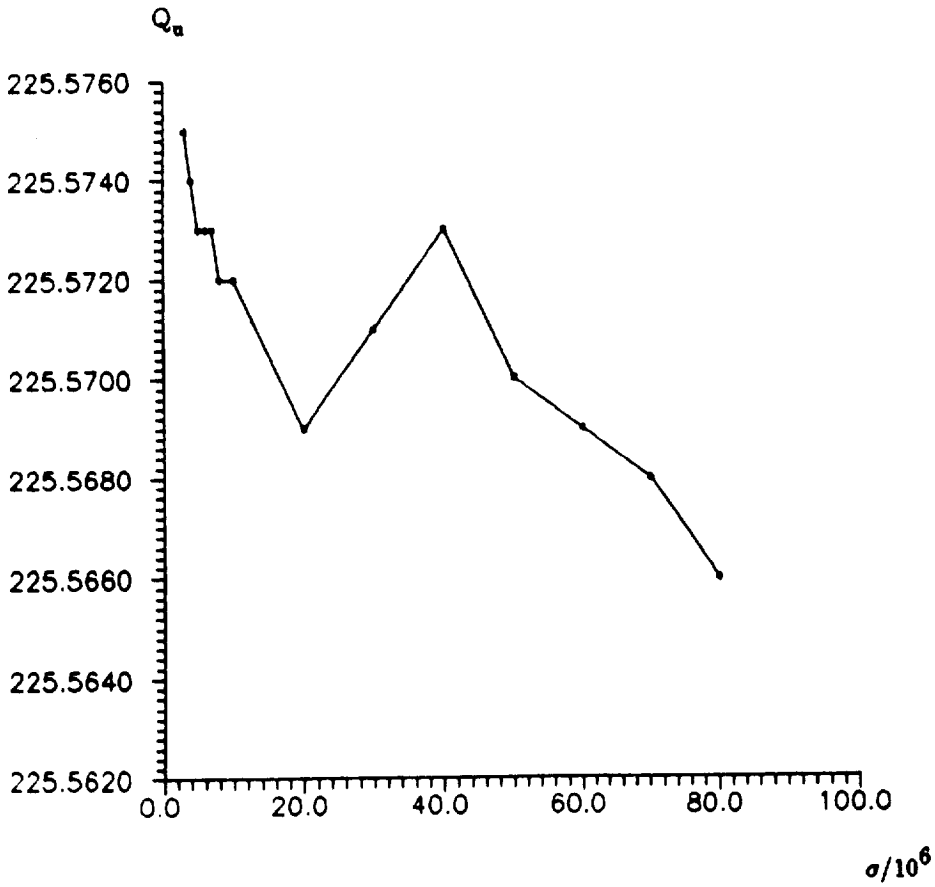

Figure 3.16 Unloaded Quality factor as a function of conductivity

Chapter 4
Summary and Conclusions

By deriving the electro-magnetic fields in and around the dielectric and establishing the linkage between the complex resonant frequency and the parameters associated with the dielectric resonator, a thorough understanding of NASA's experiment has been achieved. The derivation and illustration of the manner in which the fields propagate in the specific dielectric under study; the strength of the evanescent fields; the effect of the conductor on the resonant frequency; and how conductivity of the conductor effects the Q of the system, have given useful insight to the experiment.

The electro-magnetic fields were determined by enforcing boundary conditions of the resonator system. Section 3.3 showed that the fields at the resonators end's are predominately TE for the dielectric under consideration. This characteristic allowed for the reflection coefficient for the TE mode to be incorporated into the determination of the complex resonant frequency of the hybrid mode HEM_{111}. This determination of the relative field strength of each component has provided an understanding of how the fields propagate and are distributed in and around the dielectric. Section 3.3 also showed that at the dielectric-air interface the angle of incidence was approximately 75°, as measured from the normal.

Through this analysis, two important details regarding the design and application of the NASA experiment were revealed from the knowledge gained by deriving the evanescent fields. First, the strength of the radial evanescent fields (pg 50) determines the distance the support structure must be from the dielectric such that energy is not coupled to the support structure. Second, and more important to this experiment, an understanding of the strength and profile of

the evanescent fields at the dielectric ends was created. The profile of the evanescent fields at the resonators ends determines the distance the conductor must be from the dielectric in order to couple energy to the conductor.

Section 3.4 showed that placement of the conductor with respect to the dielectric had a dramatic effect on resonant frequency. This implied that the experimental structure must have had the ability to place different conductors at the same distance in a repeatable and accurate manner.

The last section yields insight into the goal of the NASA experiment, relating conductivity of the mesh conductor to the Q of the resonant system. Fig. 3.15 and 3.16 showed a weak relationship between the conductivity and the complex resonant frequency, suggesting only marginal usefulness of this measurement approach. In addition, the incidence angle on the conductor is not conducive to the desired near normal incident measurement.

At this point, the work remaining is an iterative process of going from the model to experimental measurements, and then back to the model. In addition, accurate measurements of the dielectric constant, dimensions of the dielectric, and accurate measurement of air gap could be incorporated into the simulation to yield more accurate simulation results. To further refine both the simulation and to redesign the experiment, the dimension of the dielectric could be chosen to cause field propagation to be more planer. This would yield stronger evanescent fields and more coupling of energy to the conductor. This would also make the approximation of the TE boundary conditions at the dielectrics end's more accurate resulting in a better simulation. Calibration of the model should be done using conductors with known conductivity such as copper.

References

[1] Courtney,W.E. "Analysis and Evaluation of a Method of Measuring the Complex Permittivityand Permeability of Microwave Insulators," **IEEE Transactions on Microwave Theory and Techniques**, Vol. MTT-18, No. 8, August 1970.

[2] Hakki, B.W. and Coleman, P.D.,"A Dielectric Resonator Method of Measuring Inductive Capacities in the Millimeter Range," **IRE Transactions on Microwave Theory and Techniques**, December 24, 1954.

[3] Wakino,K. and Nishikawa, T.,"Dielectric Resonator Materials and their Applications," **Microwave Journal, June 1987**.

[4] Itoh, T. and Rudokas, R.,"New Method for Computing the Resonant Frequencies of Dielectric Resonator," **IEEE Transactions on Microwave Theory and Techniques**, Vol. MTT-18, No. 8, January 1977.

[5] Kabayashi, Y., Aoki, T. and Kabe, Y., "Influence of Conductor Shields on the Q=Factors of a TE_0 Dielectric Resonator," **IEEE Transactions on Microwave Theory and Techniques**, Vol. MTT-18, No. 8, August 1970.

[6] Kobayashi, Y. and Tanaka, S., "Resonant Modes of a Dielectric Rod Resonator Short-circuit at Both Ends by Parallel Conducting Plates," **IEEE Transactions on Microwave Theory and Techniques**, Vol. MTT-28, No. 10, August 1986.

[7] Jaworski, M. and Pospieszalski, M.W., "An Accurate Solution of the Cylindrical Dielectric Resonator Problem, "**IEEE Transactions on Microwave Theory and Techniques**, Vol. MTT-27, No. 7, July 1979.

[8] Kajez, D. "Incremental Frequency Rule for Computing the Q-Factor of a Shield TE_{omp} Dielectric Resonator," **IEEE Transactions on Microwave Theory and Techniques**, Vol. MTT-28, No. 10, August 1986.

[9] Kajfez, D. and Hwan, E., "Q-Factor Measurement with Network Analyzer," **IEEE Transactions on Microwave Theory and Techniques**, Vol. MTT-32, No. 7, July 1984.

[10] Balanis, C.A., **Advanced Engineering Electromagnetics**, John Wiley and Sons, New York, 1989.

[11] Harrington, R.F., **Time-Harmonic Electromagnetic Fields**, McGraw-Hill Book Company, New York, 1961.

[12] Abramowitz, M. and Stegun, I., **Handbook of Mathematical Functions**, Dover Publications, INC. New York, 1972.

[13] Press, W.H., et al, Numerical Recipes, The Art of Scientific Computing, Cambridge University Press, New York, 1986.

[14] Skitek, G.G. and Marshall, S.V., **Electromagnetic Concepts and Applications**, Prentice-Hall, Inc., Englewood Cliffs, New Jersey 1982.

APPENDIX A

DERIVATION OF TE COMPONENTS IN TERMS OF H_z

The following derivation provides the components E_ϕ and H_ρ in terms of H_z for the TE_{01} mode in the dielectric resonator of Fig. 1. The derivation begins with Maxwell's curl equations.

$$\nabla \times E = -j\omega\mu H \tag{A.1}$$

$$\nabla \times H = j\omega\epsilon E \tag{A.2}$$

If (A.1) and (A.2) are expanded into cylindrical components, we obtain

$$-j\omega\mu H_\rho = \frac{1}{\rho}\frac{\partial E_z}{\partial \phi} - \frac{\partial E_\phi}{\partial z} \tag{A.3a}$$

$$j\omega\epsilon E_\rho = \frac{1}{\rho}\frac{\partial H_z}{\partial \phi} - \frac{\partial H_\phi}{\partial z} \tag{A.3b}$$

$$-j\omega\mu H_\phi = \frac{\partial E_\rho}{\partial z} - \frac{\partial E_z}{\partial \rho} \tag{A.3c}$$

$$j\omega\epsilon E_\phi = \frac{\partial H_\rho}{\partial z} - \frac{\partial H_z}{\partial \rho} \tag{A.3d}$$

$$-j\omega\mu H_z = \frac{1}{\rho}\left(\frac{\partial}{\partial \rho}(\rho E_\phi) - \frac{\partial E_\rho}{\partial \phi}\right) \tag{A.3e}$$

$$j\omega\epsilon E_z = \frac{1}{\rho}\left(\frac{\partial}{\partial \rho}(\rho H_\phi) - \frac{\partial H_\rho}{\partial \phi}\right) \tag{A.3f}$$

For the TE_{01} mode, the following components are zero:

$$E_z = 0 \qquad E_\rho = 0 \qquad H_\phi = 0$$

Eqs. (A.3) become

$$j\omega\mu H_\rho = \frac{\partial E_\phi}{\partial z} \tag{A.4a}$$

$$0 = \frac{1}{\rho}\frac{\partial H_z}{\partial \phi} \tag{A.4b}$$

$$0 = 0 \qquad \text{(A.4c)}$$

$$j\omega\epsilon E_\phi = \frac{\partial H_\rho}{\partial z} - \frac{\partial H_z}{\partial \rho} \qquad \text{(A.4d)}$$

$$-j\omega\mu H_z = \frac{1}{\rho}\frac{\partial}{\partial \rho}(\rho E_\phi) \qquad \text{(A.4e)}$$

$$0 = \frac{1}{\rho}\frac{\partial H_\rho}{\partial \phi} \qquad \text{(A.4f)}$$

Eqs (A.4b) and (A.4f) imply that H_ρ and H_z are not functions of ϕ. Setting the ϕ variation to a constant, Eqs. (A.4) simplify to

$$j\omega\mu H_\rho = \frac{\partial E_\phi}{\partial z} \qquad \text{(A.5a)}$$

$$-j\omega\mu H_z = \frac{1}{\rho}\frac{\partial}{\partial \rho}(\rho E_\phi) \qquad \text{(A.5b)}$$

and

$$j\omega\epsilon E_\phi = \frac{\partial H_\rho}{\partial z} - \frac{\partial H_z}{\partial \rho} \qquad \text{(A.5c)}$$

Taking the derivative of (A.5a) with respect to z and substituting into (A.5c) gives

$$(\omega^2\epsilon\mu + \frac{\partial^2}{\partial z^2})\, E_\phi = j\omega\mu \frac{\partial H_z}{\partial \rho} \qquad \text{(A.6)}$$

Each region must be considered separately in solving the form for (A.6). The resultant forms may then be combined to complete the problem solution. For regions, 1 and 2 of Fig. 1 we have

$$\frac{\partial^2}{\partial z^2} \Rightarrow -k_z^2\,, \qquad \text{(A.7a)}$$

in region 3 we have

$$\frac{\partial^2}{\partial z^2} \Rightarrow -\gamma^2 , \tag{A.7b}$$

and in region 4 we have

$$\frac{\partial^2}{\partial z^2} \Rightarrow \zeta^2 . \tag{A.7c}$$

We now develop the fields in each region for the TE_{01} mode, beginning with region 1. Let us define the magnetic field intensity as

$$H_z^1 = A_1 \sin k_z(z - z_o)\, J_0(k_{1\rho}\rho) , \tag{A.8a}$$

for an arbitrary z_o, where $k_{1\rho}$ is defined as

$$k_{1\rho} = \sqrt{\omega^2 \epsilon_1 \mu_1 - k_z^2} .$$

From (A.6) and (A.7a), we may write

$$E_\phi^1 = j\omega\mu_1 \frac{\partial H_z}{\partial \rho} = j\omega\mu_1 A_1 k_{1\rho} \sin k_z(z - z_o)\, J_0'(k_{1\rho}\rho) \tag{A.8b}$$

and from (A.5a)

$$H_\rho^1 = \frac{1}{j\omega\mu_1} \frac{\partial E_\phi^1}{\partial z} = k_z A_1 k_{1\rho} \cos k_z(z - z_o)\, J_0'(k_{1\rho}\rho) . \tag{A.8c}$$

In region 2 we define

$$H_z^2 = A_2 \sin k_z(z - z_o)\, K_0(jk_{2\rho}\rho) , \tag{A.9a}$$

where $k_{2\rho}$ is defined as

$$k_{2\rho} = \sqrt{\omega^2 \epsilon_2 \mu_2 - k_z^2} \, .$$

As before we may write

$$E_\phi^2 = j\omega\mu_2 A_2 k_{2\rho} \sin k_z(z - z_o) \, K_0'(jk_{2\rho}\rho) \qquad \text{(A.9b)}$$

and

$$H_\rho^2 = k_z A_2 k_{2\rho} \cos k_z(z - z_o) \, K_0'(jk_{2\rho}\rho) \, . \qquad \text{(A.9c)}$$

In region 3 we define (d = L)

$$H_z^3 = A_3 \, e^{-\gamma(z-d)} \, J_0(k_{3\rho}\rho) \, , \qquad \text{(A.10a)}$$

where $k_{3\rho}$ is defined as

$$k_{3\rho} = \sqrt{\omega^2 \epsilon_3 \mu_3 + \gamma^2} \, .$$

As before we may write

$$E_\phi^3 = j\omega\mu_3 A_3 k_{3\rho} \, e^{-\gamma(z-d)} \, J_0'(k_{3\rho}\rho) \qquad \text{(A.10b)}$$

and

$$H_\rho^3 = -\gamma A_3 k_{3\rho}\, e^{-\gamma(z-d)}\, J_0'(k_{3\rho}\rho) \,. \tag{A.10c}$$

In the last region to be considered, region 4, we define

$$H_z^4 = A_4 \sinh \zeta(z+t)\, J_0(k_{4\rho}\rho) \,, \tag{A.11a}$$

where $k_{4\rho}$ is defined as

$$k_{4\rho} = \sqrt{\omega^2 \epsilon_4 \mu_4 + \zeta^2} \,.$$

Again we write

$$E_\phi^4 = j\omega\mu_4 A_4 k_{4\rho} \sinh \zeta(z+t)\, J_0'(k_{4\rho}\rho) \tag{A.11b}$$

and

$$H_\rho^4 = \zeta A_4 k_{4\rho} \cosh \zeta(z+t)\, J_0'(k_{4\rho}\rho) \,. \tag{A.11c}$$

For simplicity of solution, a full modal expansion will not be done, but rather the fields in regions 5 and 6 will be neglected and continuity across a boundary will be applied as though the boundary were infinite. In other words, we set

$$k_{3\rho} = k_{4\rho} = k_{1\rho}.$$

We have already imposed the equality condition on k_z in regions 1 and 2.

With these approximations, Eqs. (8a) through (11c) become the following:

Region 1:

$$H_z^1 = A_1 \sin k_z(z - z_o)\, J_0(k_{1\rho}\rho)\,, \tag{A.8a}$$

$$E_\phi^1 = j\omega\mu_1 \frac{\partial H_z}{\partial \rho} = \frac{j\omega\mu_1 A_1}{k_{1\rho}} \sin k_z(z - z_o)\, J_0'(k_{1\rho}\rho) \tag{A.8b}$$

and

$$H_\rho^1 = \frac{1}{j\omega\mu_1} \frac{\partial E_\phi^1}{\partial z} = \frac{k_z A_1}{k_{1\rho}} \cos k_z(z - z_o)\, J_0'(k_{1\rho}\rho)\,. \tag{A.8c}$$

Region 2:

$$H_z^2 = A_2 \sin k_z(z - z_o)\, K_0(jk_{2\rho}\rho)\,, \tag{A.9a}$$

$$E_\phi^2 = \frac{-j\omega\mu_2 A_2}{k_{2\rho}} \sin k_z(z - z_o)\, K_0'(jk_{2\rho}\rho) \tag{A.9b}$$

and

$$H_\rho^2 = \frac{k_z A_2}{k_{2\rho}} \cos k_z(z - z_o)\, K_0'(jk_{2\rho}\rho)\,. \tag{A.9c}$$

Region 3:

$$H_z^3 = A_3\, e^{-\gamma(z-d)}\, J_0(k_{1\rho}\rho)\,, \tag{A.10a}$$

$$E_\phi^3 = \frac{j\omega\mu_3 A_3}{k_{1\rho}}\, e^{-\gamma(z-d)}\, J_0'(k_{1\rho}\rho) \tag{A.10b}$$

and

$$H_\rho^3 = -\frac{\gamma A_3}{k_{1\rho}}\, e^{-\gamma(z-d)}\, J_0'(k_{1\rho}\rho)\,. \tag{A.10c}$$

Region 4:

$$H_z^4 = A_4 \sinh \zeta(z + t)\, J_0(k_{1\rho}\rho)\,, \tag{A.11a}$$

$$E_{\phi}^{4} = \frac{j\omega\mu_4 A_4}{k_{1\rho}} \sinh \zeta(z+t)\, J_0'(k_{1\rho}\rho) \tag{A.11b}$$

and

$$H_{\rho}^{4} = \frac{\zeta A_4}{k_{1\rho}} \cosh \zeta(z+t)\, J_0'(k_{1\rho}\rho)\,. \tag{A.11c}$$

where

$$k_{1\rho} = \sqrt{\omega^2\epsilon_1\mu_1 - k_z^2}\,, \tag{A.12a}$$

$$k_{2\rho} = \sqrt{\omega^2\epsilon_2\mu_2 - k_z^2}\,, \tag{A.12b}$$

$$\gamma = \sqrt{k_{1\rho}^2 - \omega^2\epsilon_3\mu_3}\,, \tag{A.12c}$$

and

$$\zeta = \sqrt{k_{1\rho}^2 - \omega^2\epsilon_4\mu_4}\,. \tag{A.12d}$$

APPENDIX B

DERIVATION OF EIGENVALUE EQUATIONS OF SECTION 2.2

The boundary conditions for the resonator of section 2.2 are

1) $H_z^1(\rho=a) = H_z^2(\rho=a)$

2) $E_\phi^1(\rho=a) = E_\phi^2(\rho=a)$

3) $H_\rho^1(z=0) = H_\rho^4(z=0)$

4) $E_\phi^1(z=0) = E_\phi^4(z=0)$

5) $H_\rho^1(z=d) = H_\rho^3(z=d)$

6) $E_\phi^1(z=d) = E_\phi^2(z=d)$.

Applying each of these boundary conditions to the fields of App. A, we obtain the following equations:

$$A_1 \, J_0(k_{1\rho}a) = A_2 \, K_0(jk_{2\rho}a) \qquad \text{(B.1a)}$$

$$A_1 k_{2\rho} J_0'(k_{1\rho}a) = A_2 k_{1\rho} K_0'(jk_{2\rho}a) \tag{B.1b}$$

$$A_1 k_z \cos k_z z_o = A_4 \zeta \cosh \zeta t \tag{B.1c}$$

$$- A_1 \sin k_z z_o = A_4 \sinh \zeta t \tag{B.1d}$$

$$A_1 k_z \cos k_z (d - z_o) = - A_3 \gamma \tag{B.1e}$$

$$A_1 \sin k_z (d - z_o) = A_3 . \tag{B.1f}$$

Since the eigenvalues (in other words, k_z and γ) are desired in order to determine the resonant frequency, the amplitude coefficients may be eliminated from the equations to provide the simple eigen equations which must be solved. Dividing (B.1b) by (B.1a), and recalling the relationships of $k_{1\rho}$ and $k_{2\rho}$ to k_z in (A.12), we obtain an equation for k_z in terms of the frequency ω as

$$\frac{k_{2\rho} J_0'(k_{1\rho}a)}{J_0(k_{1\rho}a)} = \frac{k_{1\rho} K_0'(jk_{2\rho}a)}{K_0(jk_{2\rho}a)} . \tag{B.2}$$

An additional equation is required if we are to determine either the resonant frequency or the k_z. We may obtain such an equation by deleting A_3 and A_4 from the boundary equations also. Dividing (B.1d) by (B.1c) we obtain

$$- \tan k_z z_o = \frac{k_z}{\zeta} \tanh \zeta t \tag{B.3}$$

and dividing (B.1f) by (B.1e) we obtain

$$-\tan k_z(d - z_o) = \frac{k_z}{\gamma} . \tag{B.4}$$

The last two equations have introduced the additional variables of z_o and γ. The variable γ is defined by (A.12c). The unknown z_o may be eliminated by combining (B.3) and (B.4).

To eliminate z_o, we first expand the tangent of (B.4) using a standard trigonometric identity to obtain

$$\tan k_z(d - z_o) = \frac{\tan (k_z d) - \tan (k_z z_o)}{1 + \tan (k_z d) \tan (k_z z_o)} = -\frac{k_z}{\gamma} , \tag{B.5}$$

or

$$\tan k_z z_o = \frac{\frac{k_z}{\gamma} + \tan (k_z d)}{1 - \frac{k_z}{\gamma} \tan (k_z d)} = -\frac{k_z}{\zeta} \tanh \zeta t . \tag{B.6}$$

Eq. (B.6) may be rearranged to give

$$\tan (k_z d) = \frac{\frac{\gamma}{k_z} + \frac{\zeta}{k_z} \coth \zeta t}{1 - \frac{\gamma \zeta}{k_z^2} \coth \zeta t}$$

or

$$k_z d = \tan^{-1}\left(\frac{\gamma}{k_z}\right) + \tan^{-1}\left(\frac{\zeta}{k_z} \coth \zeta t\right) . \tag{B.7}$$

Eqs. (B.2) and (B.7) form the two equations to be solved simultaneously for the eigenvalue of the system, k_z, and thus the resonant frequency.

REPORT DOCUMENTATION PAGE

Form Approved
OMB No. 0704-0188

1. AGENCY USE ONLY *(Leave blank)*	2. REPORT DATE	3. REPORT TYPE AND DATES COVERED
	March 1994	Contractor Report

4. TITLE AND SUBTITLE
Effective Conductivity of Wire Mesh Reflectors for Space Deployable Antenna Systems

5. FUNDING NUMBERS
C NAS1-18471
TA 26
WU 233-01-03-22

6. AUTHOR(S)
William A. Davis

7. PERFORMING ORGANIZATION NAME(S) AND ADDRESS(ES)
Virginia Polytechnic Institute and State University
Bradley Department of Electrical Engineering
Blacksburg, VA 24061-0111

8. PERFORMING ORGANIZATION REPORT NUMBER

9. SPONSORING/MONITORING AGENCY NAME(S) AND ADDRESS(ES)
National Aeronautics and Space Administration
Langley Research Center
Hampton, VA 23681-0001

10. SPONSORING/MONITORING AGENCY REPORT NUMBER
NASA CR-191605

11. SUPPLEMENTARY NOTES
Langley Technical Monitor: Chase P. Hearn
Final Report

12a. DISTRIBUTION/AVAILABILITY STATEMENT
Unclassified-Unlimited

Subject Category 33

12b. DISTRIBUTION CODE

13. ABSTRACT *(Maximum 200 words)*

This report summarizes efforts to characterize the measurement of conductive mesh and smooth surfaces using proximity measurements for a dielectric resonator. The resonator operates in the HEM_{11} mode and is shown to have an evanescent field behavior in the vicinity of the sample surface, raising some question to the validity of measurements requiring near normal incidence on the material. In addition, the slow radial field decay outside of the dielectric resonator validates the sensitivity to the planar supporting structure and potential radiation effects. Though these concerns become apparent along with the sensitivity to the gap between the dielectric and the material surface, the basic concept of the material measurement using dielectric resonators has been verified for useful comparison of material surface properties. The properties, particularly loss, may be obtained by monitoring the resonant frequency along with the resonator quality factor (Q), 3 dB bandwidth, or the midband transmission amplitude. Comparison must be made to known materials to extract the desired data.

14. SUBJECT TERMS	15. NUMBER OF PAGES
microwave conductivity measurement, dielectric resonator	89
	16. PRICE CODE: A05

17. SECURITY CLASSIFICATION OF REPORT	18. SECURITY CLASSIFICATION OF THIS PAGE	19. SECURITY CLASSIFICATION OF ABSTRACT	20. LIMITATION OF ABSTRACT
Unclassified	Unclassified		